UNIVERSIDADE FEDERAL DO CEARÁ

CENTRO DE CIÊNCIAS

DEPARTAMENTO DE BIOQUÍMICA E BIOLOGIA MOLECULAR

PROGRAMA DE PÓS-GRADUAÇÃO EM BIOQUÍMICA

JACKSON LIMA AMARAL

AVALIAÇÃO DOS MECANISMOS DE AÇÃO DO PEPTÍDEO SINTÉTICO *Mo*-CBP$_3$-PEPIII CONTRA CANDIDA SPP. ATRAVÉS DE BIOQUÍMICA QUÂNTICA E SIMULAÇÕES DE DINÂMICA MOLECULAR

FORTALEZA

2019

JACKSON LIMA AMARAL

AVALIAÇÃO DOS MECANISMOS DE AÇÃO DO PEPTÍDEO SINTÉTICO *Mo*-CBP$_3$-PEPIII CONTRA *Candida spp.* ATRAVÉS DE BIOQUÍMICA QUÂNTICA E SIMULAÇÕES DE DINÂMICA MOLECULAR

Dissertação de mestrado apresentado à coordenação de do Programa de Pós-Graduação em Bioquímica como requisito obrigatório para a obtenção do título de Mestre em Bioquímica pela Universidade Federal do Ceará.
Orientador: Profa. Dra. Daniele de Oliveira Bezerra de Sousa.
Coorientador: Prof. Dr. Valder Nogueira Freire.

FORTALEZA
2019

Dados Internacionais de Catalogação na Publicação
Universidade Federal do Ceará
Biblioteca Universitária
Gerada automaticamente pelo módulo Catalog, mediante os dados fornecidos pelo(a) autor(a)

A514a Amaral, Jackson Lima.
Avaliação dos mecanismos de ação do peptídeo sintético Mo-cbp3-pepiii contra Candida spp. através de bioquímica quântica e simulações de dinâmica molecular / Jackson Lima Amaral. – 2019.
51 f. : il. color.

Dissertação (mestrado) – Universidade Federal do Ceará, Centro de Ciências, Programa de Pós-Graduação em Bioquímica, Fortaleza, 2019.
Orientação: Profa. Dra. Daniele de Oliveira Bezerra de Sousa.
Coorientação: Prof. Dr. Valder Nogueira Freire.

1. Mo-CBP3-PEPIII. 2. Mecanismos de ação. 3. Experimentação in silico. I. Título.

CDD 572

JACKSON LIMA AMARAL

AVALIAÇÃO DOS MECANISMOS DE AÇÃO DO PEPTÍDEO SINTÉTICO *Mo*-CBP$_3$-PEPIII CONTRA *Candida spp.* ATRAVÉS DE BIOQUÍMICA QUÂNTICA E SIMULAÇÕES DE DINÂMICA MOLECULAR

Dissertação de mestrado apresentado à coordenação de do Programa de Pós-Graduação em Bioquímica como requisito obrigatório para a obtenção do título de Mestre em Bioquímica pela Universidade Federal do Ceará. Área de concentração: Bioquímica Vegetal.

Aprovada em: ___/___/_____.

BANCA EXAMINADORA

_____
Profa. Dra. Daniele de O. B. de Sousa (Orientadora)
Universidade Federal do Ceará (UFC)

_____
Prof. Dr. Geancarlo Zanatta
Universidade Federal do Ceará (UFC)

_____
Prof. Dr. Bruno Lopes de Sousa
Universidade Estadual do Ceará (UECE)

_____
Dr. Pedro Filho Noronha de Souza
University of Nebraska-Lincoln

A Deus.

Espíritos de luz e familiares.

AGRADECIMENTOS

Aos órgãos financiadores CNPq, CAPES e FUNCAP, pelo apoio financeiro para o desenvolvimento deste trabalho e outros durante o período do mestrado.

À Profa. Dra. Daniele de Oliveira Bezerra de Sousa pela confiança e acreditar que podemos sair da nossa zona de conforto para produzir bons frutos e desenvolver a ciência brasileira. Agradeço por sua excelente orientação, preocupação e paciência.

Ao professor Dr. Valder Nogueira Freire pela coorientação, por ser um grande cientista inspirador e por dividir um pouco da sua criatividade quase ilimitada conosco.

Ao Dr. Pedro Filho Noronha de Souza por ter aceitado a parceria para o desenvolvimento deste projeto e por mostrar que podemos inovar mesmo dentro de conjunturas engessadas.

Ao professor Dr. José Tadeu Abreu de Oliveira pela recepção em seu grupo de pesquisa e suporte financeiro do projeto.

Ao professor participante da banca examinadora Geancarlo Zanatta por sempre estar disposto a ajudar e por todas as colaborações desde o início do trabalho. E sempre nos mostrar que o descanso também é essencial para um bom desenvolvimento científico.

Ao professor participante da banca examinadora Bruno Lopes de Sousa pelo tempo e pelas colaborações feitas ao trabalho desde a qualificação do mesmo.

Aos colegas da turma de mestrado e aos parceiros do Laboratório de Biofísica Aplicada, por estarmos unidos nos momentos de alegria e sofrimento.

À toda minha família pela motivação e apoio ao longo dos duros anos na caminhada científica.

À minha namorada Ana Brenda pelo companheirismo e entendimento por todos os sacrifícios feitos durante o mestrado.

A todos meus amigos, por todos os risos compartilhados e pelos bons momentos externos à UFC.

“Você quer passar o resto da sua vida vendendo água com açúcar ou você quer ter a chance de mudar o mundo?”

Steve Jobs.

RESUMO

Candida é o principal grupo de patógenos oportunistas em humanos e é responsável por 8 a 10% das infecções da corrente sanguínea na Unidade de Tratamento Intensivo. Foi observado um grande aumento na resistência do microrganismo as estratégias atuais, desta forma necessitando desenvolver novos fármacos com um maior espectro de ação. Os peptídeos antimicrobrianos são indicados como a alternativa mais promissora para drogas, com eficácia, um amplo espectro de ação e uma baixa indução de resistência. Baseado na proteína purificada da *Moringa oleifera* com alta atividade microbiana, *Mo*-CBP$_3$, nosso grupo de pesquisa desenhou um peptídeo antimicrobiano sintético, denominado *Mo*-CBP$_3$-PEPIII, com atividade antimicrobiana 130 vezes maior que a proteína *Mo*-CBP$_3$. Neste trabalho, demonstramos os possíveis mecanismos de ações deste peptídeo sintético através de abordagens *in silico* com enzimas chaves: esterol 14-α demetilase, proteases aspárticas secretadas, β-1,3-glucanase e membrana realística de levedura. Primeiro, analisamos as interações usando docking molecular, seguido por simulação de dinâmica molecular por 20 ns com as enzimas e 150 ns com a membrana de levedura. Finalmente, calculamos as energias de interação entre o *Mo*-CBP$_3$-PEPIII e as principais enzimas aplicando bioquímica quântica. *Mo*-CBP$_3$-PEPIII não tem interação com o sítio catalítico da esterol 1,4-alfa demetilase, apresentou interação com a protease aspártica secretada 5 e com a β- 1,3-glucanase no sítio ativo, com energia de interação de -104,9 kcal/mol e -122,2 kcal/mol, respectivamente. Através da simulação da dinâmica molecular, foi possível observar a inserção do *Mo*-CBP$_3$-PEPIII na membrana da levedura. Os resultados indicam que o mecanismo de ação do peptídeo difere dos fármacos azólicos e as interações com outras enzimas demostra possíveis mecanismos ação alternativos. Assim, pode-se inferir que o mecanismo de ação crucial é a penetração do *Mo*-CBP$_3$-PEPIII na membrana e formação de poros. O *Mo*-CBP$_3$-PEPIII tem um grande potencial para ser um novo medicamento com um amplo espectro de ação.

Palavras-chave: *Mo*-CBP$_3$-PEPIII. Mecanismos de ação. Experimentação *in silico*.

ABSTRACT

Candida is the principal group of opportunistic pathogens in humans and is responsible for 8 to 10% of the bloodstream infections at Intensive Treatment Unit. There has been observed a great increase in the microorganism resistance to current strategies, raising a necessity to develop new drugs with a greater spectrum of action. The antimicrobial peptides are indicated as the most promising drug alternative with a better cost-effective, a broad spectrum of action and a low resistance induction. Based in a purified protein from *Moringa oleifera* with high microbial activity, *Mo*-CBP$_3$, our research group designed a synthetic antimicrobial peptide, named *Mo*-CBP$_3$-PEPIII, with antimicrobial activity 130-fold higher compared to *Mo*-CBP$_3$. In this work, we demonstrated the possible mechanism of actions of this synthetic peptide through in silico approaches with keys enzymes: sterol 14-α demethylase, secreted aspartic proteases, β-1,3-glucanase and with realistic membrane of yeast. First, we analyzed the interactions using molecular docking, followed by a simulation of molecular dynamics for 20 ns with the enzymes and 150 ns with the yeast membrane. Finally, we calculated the interaction energies between *Mo*-CBP$_3$-PEPIII and the key enzymes applying quantum biochemistry. Although *Mo*-CBP$_3$-PEPIII presented no interaction with the catalytic site of sterol 1,4-alpha demethylase, it showed interaction with secreted aspartic protease 5 and β-1,3-glucanase in active site, presenting interaction energy of -104.9 kcal/mol and -122.2 kcal/mol, respectively. In the simulation of molecular dynamics was possible to observe the insertion of the *Mo*-CBP$_3$-PEPIII into the yeast membrane. Altogether, the results indicate that the mechanism of action differs from azoles drugs and the interaction with other key enzymes can be an alternative mechanism of action. Thus, it can be inferred that the mechanism of action crucial is the penetration of the *Mo*-CBP$_3$-PEPIII into the membrane and pore formation. *Mo*-CBP$_3$-PEPIII has a great potential to be a new drug with a broad spectrum of action.

Keywords: *Mo*-CBP$_3$-PEPIII. Mechanisms of action. In silico approaches.

LISTA DE FIGURAS

LISTA DE ABREVIATURAS E SIGLAS

BIRD	Binding site, Interaction energy, and Residues Domain
RMSD	Root-Mean-Square Deviation
UFC	Universidade Federal do Ceará
MFCC	Molecular fractionation with conjugate caps
MD	Molecular Dynamics
QM	Quantum Mechanics
DFT	Density Functional Theory
PDB	Protein Data Bank
SAP	Secreted Aspartic Protease
EXG	Exo-β-1,3-glucanase
POPC	1-palmitoyl-2-oleoyl-sn-glycero-3-phosphocholine
POPG	1-palmitoyl-2-oleoyl-sn-glycero-3-phosphoglycerol
CHL	Cholesterol
DOPC	1,2-dioleoyl-sn-glycero-3-phosphocholine
POPE	1- palmitoyl-2-oleoyl-sn-glycero-3-phosphoethanolamine
POPS	1-palmitoyl-2-oleoyl-sn-glycero-3-phospho-L-serine
POPA	1-palmitoyl-2-oleoyl-sn-glycero-3-phosphate
DPPC	1,2-dipalmitoyl-sn-glycero-3-phosphocholine

SUMÁRIO

1 CAPÍTULO I - REFERÊNCIAL TEÓRICO

1.1 *Candida spp.*

Espécies de *Candida* são fungos oportunistas, sendo a maior causa de morte de pacientes imunossuprimidos no mundo, o que representa um sério problema de saúde pública (Pappas *et al.,* 2016). Candidemia é a infecção hospitalar mais frequente e responsável por mais de 15% de todas as infecções sanguíneas, se considerar apenas infecções causadas por fungos, sendo as diferentes espécies de *Candida* responsáveis por 50 a 70% dessas infecções (Barchiesi *et al.,* 2016).

Candida albicans é a espécie mais encontrada quando se isola os agentes causadores das infecções, porém outras espécies, como *C. parapsilosis, C. tropicalis, C. krusei, C. glabrata* e *C. famata* têm aumentado significativamente seus índices de infecções, principalmente quando em pacientes imunodeprimidos tais como aqueles portadores do vírus HIV (Patil *et al.,* 2015; Barchiesi *et al.,* 2016).

Espécies de *Candida* apresentam uma grande flexibilidade em seus modos de vida, sendo capaz de crescer em ambientes extremamente diferentes, no que se refere a disponibilidade de nutrientes, variação de temperatura, pH, osmolaridade e a quantidade de oxigênio disponível (Paramythiotou *et al.,* 2014). Esse fato associado ao grande desenvolvimento de resistência das leveduras pelos antifúngicos já descobertos, bem como a capacidade de formar biofilmes com outras espécies, torna o genêro *Candida* um sério risco para a saúde humana, sendo necessário o desenvolvimento contínuo de novas drogas com diferentes mecanismos de ação para se garantir um eficiente tratamento aos pacientes (Álvares *et al.,* 2007; Shoham and Marr, 2012).

1.2 Antifúngicos tradicionais e seus mecanismos de ação

A classe dos antifúngicos azóis é a principal e mais utilizada no mercado atual. Antifúngicos desta classe possui ação direta no metabolismo do ergosterol dos fungos, especificamente através da inibição da enzima lanosterol 14-α-demetilase, a qual é responsável pela transformação do lanosterol em ergosterol. Desta forma, sem o ergosterol presente, a membrana fúngica desestabiliza, o que leva a inibição do crescimento fúngico e acúmulo de compostos tóxicos no meio intracelular,

ocorrendo, posteriormente, a morte celular. O principal representante do grupo dos azois é o flucanazol, sendo a droga de escolha para a maioria das infecções por *Candida.* Além disso, é o antifúngico mais recomendado devido ao seu baixo custo. Apesar dos azóis possuírem vários benefícios e serem bem tolerados, possuem efeitos adversos como hepatotoxicidade e um aumento no número de cepas resistentes (Paramythiotou *et al.,* 2014; Nett and Andes, 2016).

Outros medicamentos foram desenvolvidos para a inibição da biossíntese do ergosterol, como as alilaminas e tiocarbamatos, porém ainda são pouco utilizados devido aos seus efeitos adversos.

Os polienos representam a segunda classe de antifúngicos mais utilizada. Esta classe possui ação direta na membrana fúngica, através da interação com o ergosterol, o que causa uma perturbação na estrutura da membrana promovendo extravasamento de componentes intracelulares e a consequente morte celular. As principais drogas desta classe são a anfotericina B e a nistatina, as quais são utilizadas para pacientes em casos extremos de risco de morte. Isto porque esses fármacos apresentam alta toxicidade, sobretudo sobre os rins, sendo este um fator que limita o uso (Mesa-Arango *et al.,* 2012).

A flucitosina representa outra classe de antifúngico, a qual é uma análoga das bases nitrogenadas pirimidinas, possuindo mecanismo direto na inibição da síntese de ácido nucleico. Em uso clínico, é preferível utilizá-la em conjunto com a anfotericina B para casos extremos, devido aos seus diversos e fortes efeitos colaterais, bem como uma rápida ocorrência de resistência (Nett; Andes, 2016; Prasad *et al.,* 2016).

Griseofulvina é um inibidor da mitose fúngica que age através da interferência da produção de microtúbulos e perturbação da formação do fuso mitótico. O principal problema relacionado a este composto é a falta de especificidade, logo apresentando atividade citotóxica (Francois *et al.,* 2005).

Uma nova classe de antifúngicos foi descoberta recentemente e classificada como equinocandinas. São moléculas capazes de perturbar a formação e organização da parede celular fúngica. Seu principal mecanismo de ação é através da inibição das enzimas responsáveis pela organização da parede celular tais como a β-1,3-glucano sintase e β-1,3-glucanase. Como consequência, há o enfraquecimento da parede celular e incapacidade da célula resistir aos estresses osmóticos. A principal vantagem desta classe é o número restrito de efeitos

adversos, visto que as células animais não possuem parede celular. As equinocandinas são utilizadas, preferencialmente, em casos de resistências aos azóis (Maubon *et al.,* 2014; Paramythiotou *et al.,* 2014).

Inibidores das proteases aspárticas secretadas (SAPs) atualmente vêm sendo indicada como candidatos para o desenvolvimento de novas drogas, visto que as SAPs são responsáveis por várias funções para a célula fúngica, como nutrição, adesão as células humanas e formação de biofilmes. As SAPs são 10 isoenzimas com diferentes funções, cada uma e expressadas em diferentes momentos. A SAP 5, por exemplo, é apontada como a maior responsável pela adesão fúngica e formação de biofilmes sendo o principal alvo para o desenvolvimento de novas drogas (Mathé; Van Dijck, 2013; Silva *et al.,* 2019).

1.3 Peptídeos antimicrobianos

Os peptídeos antimicrobianos (PAMs) são oligopeptídeos que possuem de 5 a 50 aminoácidos e são moléculas de defesa encontradas em diversos organismos. Os PAMs possuem ação principalmente na permeabilização da membrana de microrganismos através de interações iônicas e hidrofóbicas com os fosfolipídios presentes em sua estrutura (Yang *et al.,* 2018).

Apesar de se observar diferentes tipos de estruturas secundárias para esses peptídeos, é mais relatado na literatura a estrutura em formato de alfa-hélice. Além disso, essas moléculas são catiônicas devido a predominância de aminoácidos carregados positivamente, o que possibilita as interações com os fosfolipídios aniônicos. Mesmo com a membrana sendo o alvo mais provável dos PAMs é observado que esses peptídeos também possuem alvos intracelulares e extracelulares (Lum *et al.,* 2015).

Apesar de PAMs naturais estarem sendo comercializados, há vários entraves, como o seu alto custo e a sua grande citotoxicidade (Mahlapuu *et al.,* 2016). Recentemente, os PAMs sintéticos têm sido considerado a alternativa mais promissora para o desenvolvimento de novos fármacos, visto seu grande espectro de ação, baixa indução de resistência e baixa citotoxicidade (Cardoso *et al.,* 2018). Os PAMs sintéticos também possuem uma grande vantagem comercial comparado aos PAMs naturais e às novas drogas disponíveis, pois o tempo necessário para serem comercializados é menor (Fosgerau *et al.,* 2014). PAMs sintéticos podem ser

formulados *de novo*, ou seja, sem se basear em proteínas já existentes com atividades antimicrobianas, bem como podem ser desenhados bioinspirados em fragmentos de proteínas com grandes atividades antimicrobiana. Diversos *softwares* estão disponíveis online e com acesso gratuito, que através de cálculos de alinhamento com outros peptídeos com atividade comprovada e baseando-se na hidrofobicidade e nas cargas de pequenas sequências são capazes de inferir possível PAMs sintéticos com atividade antimicrobiana.

1.4 Mo-CBP3-PEPIII

Nosso grupo de pesquisa recentemente desenhou um peptídeo sintético inspirado em um fragmento de proteína ligante a quitina presente em sementes de *Moringa oleifera* denominada *Mo*-CBP$_3$, que apresenta uma grande atividade antimicrobiana incluindo as leveduras do gênero *Candida* (Freire *et al.,* 2015; Batista *et al.,* 2014). Apesar de promissora, a produção de *Mo*-CBP$_3$ em larga escala apresenta custo elevado o que dificulta sua utilização como uma droga antifúngica. Assim, foram desenhados os peptídeos *Mo*-CBP$_3$-PEPI, *Mo*-CBP$_3$-PEPII e *Mo*-CBP$_3$-PEPIII baseados na sequência aminoacídica da referida proteína. Todos os peptídeos apresentaram atividade contra Candida, porém o *Mo*-CBP$_3$-PEPIII apresentou maior atividade que os outros (Oliveira *et al.,* 2018). *Mo*-CBP$_3$-PEPIII apresenta um CIM90%, ou seja, uma concentração mínima inibitória do crescimento fúngico em 90%, de 4,4 e 2,2 µM para *Candida albicans* e *C. parapsilosis*, respectivamente e CIM50% de 17,5 e 2,2 µM para *C. krusie* e *C. tropicalis,* respectivamente. Através desses resultados pode-se observar o grande potencial desse peptídeo tornar-se uma nova droga antifúngica.

A fim de observar os possíveis efeitos adversos do peptídeo *Mo*-CBP$_3$-PEPIII, foram realizados experimentos de atividade hemolítica e avaliação de sua toxicidade para células humanas. Foi observado que esse peptídeo não se mostrou tóxico sendo provavelmente mais segura que alguns medicamentos que são utilizados em casos avançados de candidemia, como a anfotericina B.

No mesmo trabalho de Oliveira e colaboradores (2018), os autores verificaram a formação de poros de 20 kDa na membrana da levedura *C. parapsilosis*. Essa espécie foi escolhida no referido trabalho devido ao aumento dos casos de doenças oriundos desta levedura e seu aumento na resistência contra

alguns antifúngicos tradicionais. Além da formação dos poros, outros alvos intra- e extracelulares não são descartados visto o amplo espectro de ação dos peptídeos antimicrobianos.

1.5 Métodos computacionais

Diversos métodos computacionais estão disponíveis para o estudo de ligantes com proteínas alvo, bem com membranas. Entre os métodos mais utilizados pode-se citar o Docking ou Ancoramento molecular e Simulação de Dinâmica Molecular. Cálculo quântico é menos utilizado, porém é uma poderosa ferramenta com maior precisão e eficácia no estudo de interações entre ligante e proteína, bem como proteína com proteína. Esses métodos permitem simular eventos físicos em escala atomística muito aproximados ao que de fato acontece em meios biológicos (Sousa *et al.,* 2016; Zanatta *et al.,* 2016).

Através do método de Docking Molecular é possível observar as interações entre um ligante com uma proteína. No caso específico desse trabalho, pretendeu-se observar a interação entre algumas proteínas alvo existentes nas leveduras com o peptídeo *Mo*-CBP$_3$-PEPIII. Esse método é tanto qualitativo como quantitativo, visto que é possível analisar as possíveis regiões de interação da proteína com o ligante, sendo gerado um score do docking em termos de energia livre em kcal/mol para cada interação. Para que se observe o maior número de interações possíveis, utiliza-se o docking flexível, ou seja, mantem-se todas as ligações do ligantes capazes de rotacionar livres, desta forma, o software analisa cada rotação das ligações, o que leva a uma conformação diferente do ligante logo diferentes poses em diferentes regiões são analisadas e as mais prováveis são indicadas pelas menores energias. As melhores poses obtidas no Docking são analisadas e utilizadas como entradas para as simulações de dinâmica molecular (Trott and Olson, 2010).

Dinâmica molecular se baseia em funções de energia potencial simples, como oscilador harmônico e potenciais Coulombianos para a modelagem de sistemas moleculares. Através das simulações de dinâmica molecular pode-se observar os movimentos atômicos de diferentes sistemas. Geralmente, utiliza-se uma caixa d'água, como o próprio nome já diz é verdadeiramente uma caixa d'água em escalas nanométricas, na qual o sistema a ser estudado fica em seu interior com

íons para simular condições de pH, pressão e temperatura dos sistemas biológicos ao longo do tempo. Diversos estudos em diferentes áreas têm utilizado essa técnica, podendo-se citar estudos com bioquímica estrutural, biofísica, biologia molecular, enzimologia e biotecnologia. É muito aplicada para o desenvolvimento de novas drogas, visto que se pode observar a interação das drogas com diferentes alvos em sistemas próximos do real, através simulação de movimentos possíveis nos sistemas (Phillips et al., 2005; Lyu *et al.,* 2015).

A bioquímica quântica a cada ano é mais aplicada com o objetivo de entender como ocorre as interações moleculares, bem como quantificar as energias destas interações. Diversos estudos já foram publicados envolvendo a interação de proteína com ligantes, bem como proteínas com ligantes. Atualmente, bioquímica quântica é possível através da aplicação da Teoria do Funcional da Densidade (DFT), nessa teoria utiliza-se a densidade eletrônica com base para os cálculos, levando em conta apenas três coordenadas espaciais dos elétrons. Cálculos mais rápidos só foram possíveis após o desenvolvimento dessa teoria, visto que se os cálculos fossem baseados diretamente na função de onda iriam ter um custo computacional e temporal muito grande (Zhang e Zhang, 2003; Chen, Zhang e Zhang, 2005).

Com a bioquímica quântica pode-se analisar a interação de cada resíduo do sítio ativo da proteína com o ligante, bem como inferir a energia de interação total, assim sendo possível determinar os melhores ligantes, bem como mecanismos de ação de cada ligantes através de uma abordagem molecular. Também é possível sugerir mutações pontuais para incrementos nas energias de interação e assim sendo possível o aumento da atividade, dependendo do sistema (Rodrigues *et al.,* 2013; Sousa *et al.,* 2016; Zanatta *et al.,* 2016).

1.6 Justificativa

Sendo o peptídeo *Mo*-CBP$_3$-PEPIII um forte candidato para a formulação de uma nova droga, com diversas vantagens aos medicamentos presentes no mercado para o tratamento de *Candida spp.* faz-se necessário o estudo dos possíveis mecanismos de ação desse peptídeo. Com abordagens precisas e eficientes *in silico*, como docking molecular, simulações de dinâmica molecular e bioquímica quântica é possível analisar as possíveis interações do *Mo*-CBP$_3$-PEPIII

com os alvos das drogas já utilizadas, bem como compreender a forma de inserção desse peptídeo em membranas fúngicas. Desta forma, este trabalho visa a aplicação dos métodos computacionais para o entendimento dos mecanismos de ação do *Mo*-CBP_3-PEPIII.

2 CAPÍTULO II - INSIGHTS INTO MODES OF ACTION OF THE SYNTHETIC PEPTIDE *MO*-CBP$_3$-PEPIII AGAINST CANDIDA SPP. THROUGH QUANTUM BIOCHEMISTRY AND MOLECULAR DYNAMICS SIMULATION

2.1 Introduction

Candida spp. is the most important human pathogen yeast responsible for invasive candidiasis, which is a major cause of human mortality in immunosuppressed patients (SCHNEIDER *et al*., 2018; QUINDÓS, 2016). Nowadays, it is estimated that Candida is responsible for 8 to 10% of bloodstream infection at Intensity Treatment Unit (ITU) and at least 50% of these are caused by *Candida albicans* (Negri *et al.,* 2010; Mayer, Wilson e Hube, 2013). Recently, it was noticed cases of candidiasis caused by other candida species, such as *C. krusei* and *C. parapsilosis*, which showed resistance toward conventional treatments available (Puig, 2014; Berkow *et al.,* 2017).

Up to date, there are at least three important classes of antifungal drugs: azoles, echinocandins and polyenes. The azoles bind lanosterol 14 α-demethylase (CYP51) leading to inhibition of the ergosterol synthesis. The echinocandins inhibit the 1,3-β-glucan synthase, which impairs in normal formation of cell wall. Polyenes interact with the sterols present in the fungi membrane, increasing the membrane permeability and causing the leakage and cell death. The resistance to common antifungal drugs suggests that in a few years the current strategies to treat diseases caused by *Candida* species will be inefficient. Therefore, the development of new active molecules holding a different mechanism of action from known drugs is quite important to continue obtaining successful treatments (Czaplewski *et al.,* 2016).

Based on that, many researchers worldwide are searching for new alternative molecules. Among them, antimicrobial peptides (AMPs) present a great unexplored potential. AMPs are ubiquitous oligopeptides containing 5 to 50 amino acids that act as defense molecules. AMPs present a wide-spectrum of action, low rates of resistance induction, and are non-cytotoxicity to the host. For these reasons several studies have presented AMPs as potential molecules to be used in development of new drugs (Fjell et al., 2012; Cardoso et al., 2018). However, natural AMPs present some limitations such as low resistance to proteolysis, high purification cost followed by low yield and sometimes toxicity for the host. Given that, synthetic

antimicrobial peptides (sAMP) derived from natural AMP have received more attention as alternative to produce new drugs.

Recently, our research group developed a sAMP named *Mo*-CBP$_3$-PEPIII (Oliveira et al., 2018) that presents a MIC90% at low concentration of 4.4 and 2.2 µM to *Candida albicans*, *C. parapsilosis*, respectively, and MIC50% of 17.5 and 2.2 µM *C. krusie* and *C. tropicalis,* respectively. In addition, *Mo*-CBP$_3$-PEPIII did not exhibit hemolytic or toxic activity to mammalian cells. Also, the author verified a 20-kDa-pore *C. parapsilosis* membrane, which indicates that this is a target of *Mo*-CBP$_3$-PEPIII against this microorganism, however intra- and extracellular targets are not discarded. For instance, recent studies with antimicrobial peptides indicate that secreted aspartic proteases (SAPs), responsible to provide nutrients to pathogen propagation, cell adhesion, and cell wall maintenance are also targets of AMPs (HANCOCK *et al.,* 2006; LUM *et al.*, 2015; IKONOMOVA *et al.,* 2018)

Synthetic AMPs are designed to form pores in the fungi membrane. Then, interaction studies of AMPs with membranes via molecular dynamics can provide very interesting insights to understand their mechanism of action. A new approach by using realistic membranes simulation is a very powerful technique to address the membrane complexity and its variety of components. The results obtained in this study will provide specific insights into mechanism of action of *Mo*-CBP$_3$-PEPIII and its interaction with key enzymes and biomimetic membrane.

2.2 Materials and methods

2.2.1 Structural Data

All structural analysis were performed by using data from X-ray crystal structure analysis of sterol 14-alpha demethylase (CYP51) (PDB ID: 5V5Z), secreted aspartic proteinase (Sap) 1 (PDB ID: 2QZW), secreted aspartic proteinase (Sap) 5 (PDB ID: 2QZX) and exo-β-(1,3)-glucanase (EXG) (PDB ID: 1CZ1) (CUTFIELD *et al.,* 1999; BORELLI *et al.,* 2008). The protonation state of all receptors and peptide *Mo*-CBP$_3$-PEPIII were adjusted according to data obtained from the PROPKA 3.1 web server tool (http://propka.ki.ku.dk/) and from the Protonation tool in Discovery Studio package.

2.2.2 Molecular Docking

Molecular docking was performed with Autodock Vina, version 1.1.2, which uses the efficient quasi-Newton method, and Broyden–Fletcher–Goldfarb–Shanno (BFGS) for local optimization (TROTT and OLSON, 2010). The Autodock graphical interface, AutoDockTools, version 1.5.6, was used to retain polar hydrogens and add partial charges to the proteins and ligands using the Kollman united charges (SOUSA *et al.,* 2016). The receptors (Sap 1 and 5, CYP51 and EXG) and ligand (*Mo*-CBP$_3$-PEPIII) were treated as rigid and flexible molecules, respectively. The grid box was defined by a 60 Å x 60 Å x 60 Å cube with the receptors in the center. Exhaustiveness was set up to 15, and all other parameters were used as default. For each receptor, the ten peptide conformation top-ranked based on the predicted binding affinity (in kilocalories per mole [kcal mol^{-1}]) were analyzed. The solutions were first chosen based on the coordination of the crystal structure for the original ligands, and then the most suitable results were further ranked based on the theoretical binding energy (given as a negative score in kcal mol^{-1}).

2.2.3 Molecular Dynamics

Molecular Dynamics (MD) simulations were performed using NAMD v. 2.12, adopting the TIP3 water model and the CHARMM27 force field, which has specific parameters for all amino acids (PHILLIPS *et al.,* 2005). Chloride and sodium counter ions were added to neutralize the system maintaining a final salt concentration of 0.15 mol/L. The simulation was performed with minimization of 1 000 steps, after the system was equilibrated and the temperature of the system was adjusted from 100 K to 300 K followed by simulation of 20 ns with a time step of 2 fs. The RMSD code evaluated the distance root-mean-square deviations of the ligand and the receptor amino acid residues.

2.2.4 Molecular Fractionation with Conjugate Caps (MFCC)

A detailed energetic description of the interaction between the receptors with *Mo*-CBP$_3$-PEPIII was performed by quantum mechanics calculations. For this purpose, the MFCC scheme was applied, which is a very useful approach that

provides an accurate description of biological systems through quantum calculations (ZHANG and ZHANG 2003; HE and ZHANG, 2005; CHEN, ZHANG and ZHANG, 2005). A method modified by Rodrigues and co-workers (2016) was applied to describe protein–peptide interactions; the interaction energy between two specific residues (Ri and Rj) was calculated as follows:

$$E_I(R_i–R_j) = E(C_{i-1}R_iC_{i+1}C_{j-1}R_jC_{j+1}) - E(C_{i-1}R_iC_{i+1}C_{j-1}C_{j+1}) – E(C_{i-1}C_{i+1}C_{j-1}R_jC_{j+1}) + E(C_{i-1}C_{i+1}C_{j-1}C_{j+1}) \quad (1)$$

Where, the C_k terms refer to the conjugate caps, which was carefully chosen to reproduce the local electronic environment of the amino acid residues (WU et al., 2007). In our study, these caps are the residues covalently bound to R_k; $C_{k\pm1}$ = $R_{k\pm1}$ plus hydrogen atoms placed at any dangling bonds. At the right-hand side of eqn (1), the first term, $E(C_{i-1}R_iC_{i+1}C_{j-1}R_jC_{j+1})$, is the total energy of the system formed by two interacting capped residues. The second term, $E(C_{i-1}R_iC_{i+1}C_{j-1}C_{j+1})$, gives the total energy of the system formed by the capped residue R_i and the hydrogenated caps of R_j. The third term, $E(C_{i-1}C_{i+1}C_{j-1}R_jC_{j+1})$, is the total energy of the system formed by R_j and the set of caps of R_i. Finally, $E(C_{i-1}C_{i+1}C_{j-1}C_{j+1})$ is the total energy of the system formed by the caps only.

Following this scheme, structural files (PDB format) were prepared and used as input for calculations with DMOL3 code (DELLEY, 2000). The total energies obtained for each system were then inserted in the above equation to determine the interaction energy between a specific pair of amino acid residues.

2.2.5 The BIRD Panel

The energy contribution of all interactions protein-protein involved in the *Mo*-CBP$_3$-PEPIII – receptors complex, as well as the individual contributions of specific amino acid residues, are plotted in BIRD panels – an acronym for Binding site, Interaction energy and Residues Domain. The BIRD panel depicts: (i) the interaction energy (in kcal mol^{-1}) between a specific pair of residues (or the energetic contribution of an specific amino acid residue), employing horizontal bars, from which one can assess the importance of each interaction/residue in the complex formation, whether attractive (negative energy) or repulsive (positive energy); (ii) the binding interface radius to which each interaction/residue belongs, at the right side; and (iii) the molecules of water involved in the interaction (ZANATTA et al., 2016).

2.2.6 Energy Stabilization

The energy contributions of all the interactions between the *Mo*-CBP_3-PEPIII and the receptors were computed, considering a distance-based activity site. For this purpose, all *Mo*-CBP_3-PEPIII residues placed at a maximum distance of 5.0 Å from the receptors activity site were initially identified and then used as a reference for mapping an imaginary sphere of 5.0 Å using the software Discovery Studio. Afterwards, all residues of the receptors with at least one atom present inside the sphere was selected, thus determining all pairs of interacting residues in the complex. The selected top distance was based on an average estimate that takes into account the fact that variations of interactions energy in protein systems tend to become negligible at distances higher than 5.0 Å (SOUSA *et al.,* 2016).

2.2.7 Mo-CBP_3-PEPIII - Yeast Mimics Membrane System

The yeast membrane system was built containing the same components as that employed by Balliano and co-workers (1999), consisting of 1,2-dioleoyl-sn-glycero-3-phosphocholine (DOPC), 1-palmitoyl-2-oleoyl-sn-glycero-3-phosphoethanolamine (POPE), 1-palmitoyl-2-oleoyl-sn-glycero-3-phosphate (POPA), 1-palmitoyl-2-oleoyl-sn-glycero-3-phospho-L-serine (POPS), 1,2-dipalmitoyl-sn-glycero-3-phosphocholine (DPPC), and cholesterol. The initial *Mo*-CBP_3-PEPIII-membrane systems were constructed based in the work of Lyu and co-workers (2018), which used CHARMM-GUI's Membrane Builder module (JO *et al.,* 2007; WU et al., 2014; LEE *et al.,* 2019). A 3 nm minimum height of water was added on both at the top and the bottom of the system to simulate a fully hydrated bilayer system. A 0.15 M of Na^+ and Cl^- salts (both potassium and chloride were added) concentration was set by mimicking the physiological conditions and the final system was neutral in charge. The simulation was performed with NAMD 2.12 to observe the insertion of *Mo*-CBP_3-PEPIII in the lipid bilayer membrane. Initially, it was performed a minimization of 10 000 steps, followed by a simulation of 150 ns with a time step of 2 fs (KIM, IYER and IM, 2008; BROOKS *et al*., 2009; LEE *et al.,* 2016).

2.3 Results and Discussion

2.3.1 Molecular Docking

The analysis showed that *Mo*-CBP$_3$-PEPIII interacts with the sterol 14α-Demethylase (CYP51) of *C. albicans* in different regions (Figure 1). The score of the molecular docking varies between -5.1 and -6.1 kcal/mol depending on the region. *Mo*-CBP$_3$-PEPIII does not interact with the CYP51 active site, which is marked by a yellow and dashed circle in Figure 1. This result indicates a different mechanism presented by *Mo*-CBP$_3$-PEPIII compared to azoles, which is supported by strongly interaction with active site of CYP51 avoiding the formation of ergosterol, an important component of *C. albicans* membranes.

Mo-CBP$_3$-PEPIII interacts with the secreted aspartic proteases (SAP) as summarized in Figure 2. Molecular Docking revealed that *Mo*-CBP$_3$-PEPIII interacts at the active site of SAP1 and SAP5, with small distances of catalytic residues, which is a different mechanism when compared to CYP51. Regarding to SAP1, the *Mo*-CBP$_3$-PEPIII presented a score of of -5.7 kcal/mol and a distance of 3.5 Å and 4.1 Å of catalytic residues Asp32 and Asp218, respectively, as shown in Fig. 2A. The score of the interaction between SAP5 and *Mo*-CBP$_3$-PEPIII was -7.4 kcal/mol suggesting a higher attraction of the *Mo*-CBP$_3$-PEPIII by SAP5 than by SAP1. In addition, distances between the catalytic residues of SAP5 to the *Mo*-CBP$_3$-PEPIII were also lower: 2.4 Å and 3.2 Å for Asp32 and Asp218, respectively (Figure 2B). Lum and co-workers (2015) obtained similar results by comparing the score of the docking of four different peptides with potential to inhibit the SAP1 and SAP5. *Mo*-CBP$_3$-PEPIII has a greater potential to inhibit SAP5 then SAP1. As such, SAP5 was used to further studies about simulation of molecular dynamics and quantum calculus.

Mo-CBP$_3$-PEPIII presented a score of molecular docking of -7.0 kcal/mol to exo-β-(1,3)-glucanase (EXG) and interacts with the catalytic residues with a distance of 2.0 Å and 2.4 Å in relation to Glu192 and Glu292, respectively (Figure 3). This result indicates a large energy of attraction between Mo-CBP3-PEPIII and EXG, suggesting a strong inhibitory potential of Mo-CBP3-PEPIII toward to EXG.

Figure 1. Interactions between *Mo*-CBP$_3$-PEPIII and sterol 14α-demethylase (CYP51). *Mo*-CBP$_3$-PEPIII is represented as a stick and sphere colored in cyan. CYP51 is represented as a surface colored in light blue. The yellow circle mark the binding site position.

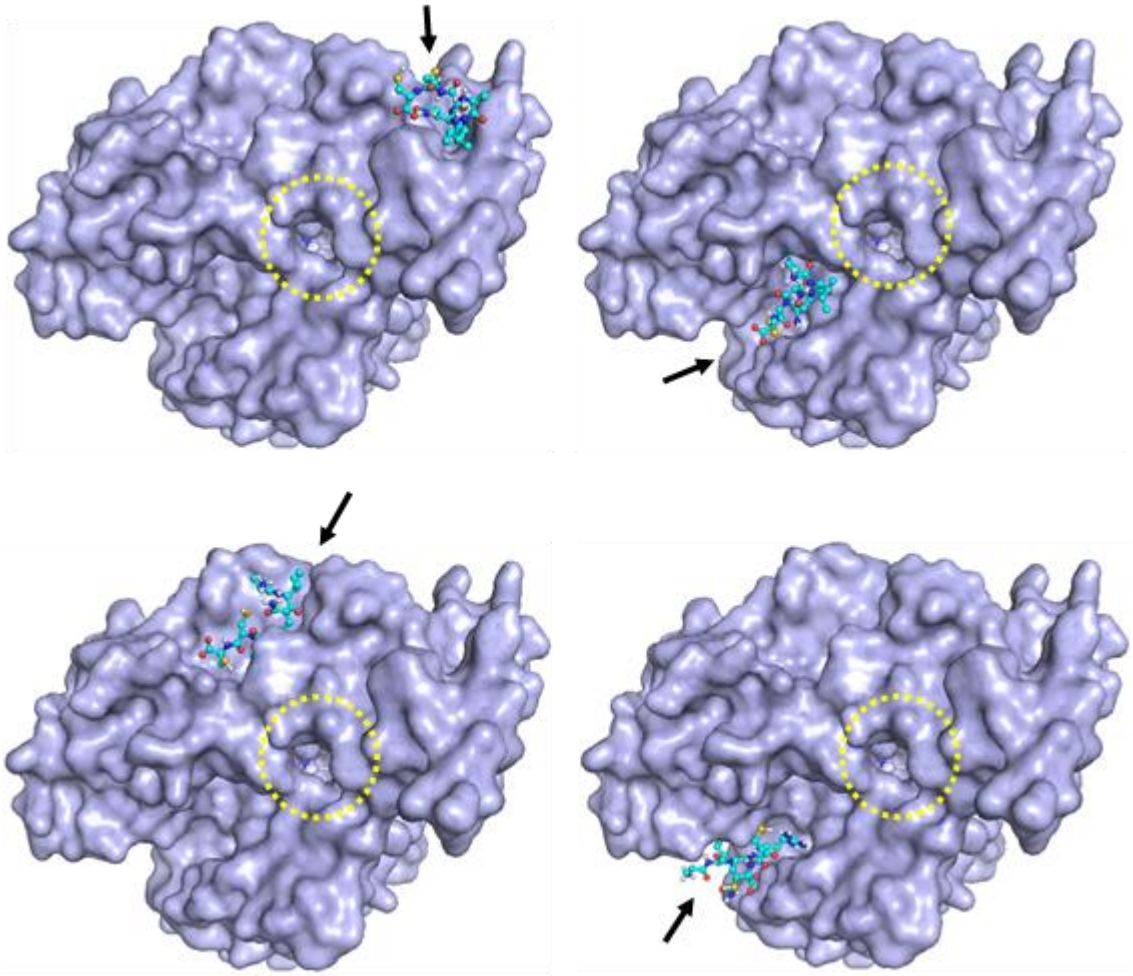

Source: Prepared by the author

Figure 2. Interaction between *Mo*-CBP$_3$-PEPIII and secreted Aspartic Proteases. (A) Interaction with the secreted aspartic protease 1 (PDB ID 2QZW) with docking score of -5.7 kcal/mol; (B) Interaction with the secreted aspartic protease 5 (PDB ID 2QZX) with docking score of -7.4 kcal/mol. The catalytic residues Asp218 and Asp32 of the enzymes are represented in stick. The dashed lines represent the distance in Å (small numbers) between the catalytic residues and *Mo*-CBP$_3$-PEPIII. *Mo*-CBP$_3$-PEPIII is represented as a stick and sphere colored in cyan.

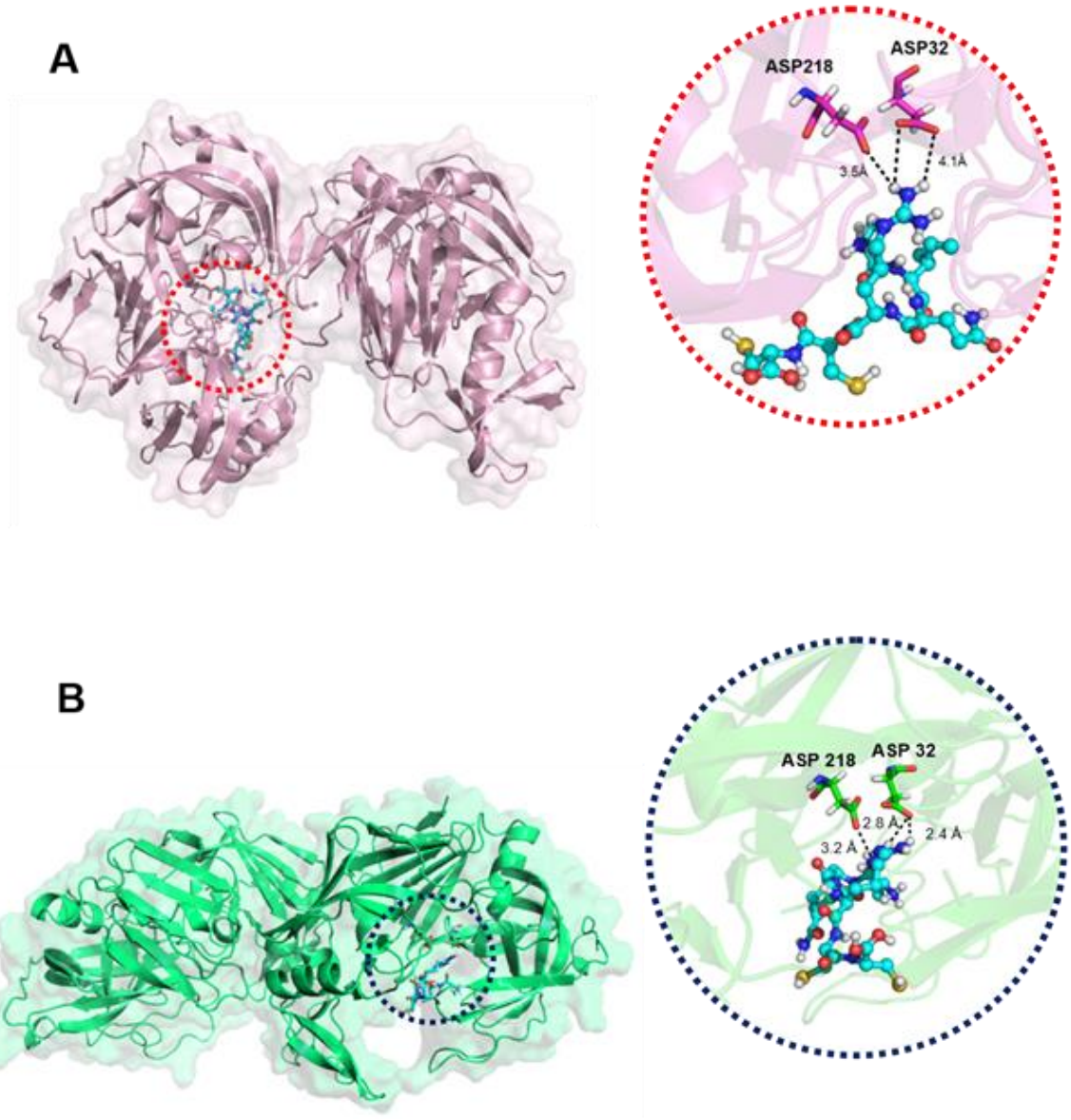

Source: Prepared by the author

2.3.2 Molecular Dynamics

Aiming to evaluate the behavior of *Mo*-CBP$_3$-PEPIII-EXG and *Mo*-CBP$_3$-PEPIII -SAP5 complexes over time and obtain a steady structure in conditions close to reality, was performed a simulation of molecular dynamics of the referred complexes.

During 20 ns of simulation of molecular dynamics, was noticed the complexes are stabilized from approximately 12.5 ns (Figure 4). After stabilization of the complexes, was possible to observe differences of less than 0.2 Å in RMSD. Also, It is possible to observe the complex *Mo*-CBP$_3$-PEPIII -SAP5 showed a greater variation of RMSD from the initial moment until the moment in which the complex stabilizes, which had a variation of approximately 2.4 Å, while the complex between *Mo*-CBP$_3$-PEPIII and EXG presented a variation of 1.7 Å.

2.3.3 Interaction between Mo-CBP$_3$-PEPIII and SAP5

The BIRD panel presents the main energies of interaction between the residues of the enzyme and ligands, as well as the water molecules involved in the interaction and the distances between the residue and the ligand. The best residue to *Mo*-CBP$_3$-PEPIII-SAP5 interaction is the Asp86, which presents an energy of -28.3 kcal/mol and three water molecules favoring hydrogen bridges formation (Figure 5). The SAP-5 Asp86 interact with *Mo*-CBP$_3$-PEPIII Ala1 and Ile2 present in the peptide with interaction energies of -15.6 and -9.7 kcal/mol, respectively, as shown in Figure 6A. The distance of the interaction between Asp86 and Ala1, as well as the Ile2 is 4.1 Å.

The second most important residue to the interaction with the SAP5 is the Trp51, which presents an attractive energy of -19 kcal/mol and radius of 2.5 Å away from *Mo*-CBP$_3$-PEPIII (Figure 5). Trp51 has interaction energies of -5.0, -2.0, -6.0, -5.0 and -1.0 kcal/mol for Ile2, Gln3, Arg4, Cys5 and Cys6 *Mo*-CBP$_3$-PEPIII amino acids, respectively. Thus, the strong interaction of this residue with the peptide is caused by the various small energies of interaction that have distances of 2.8, 3.8 and 3.1 Å of the residues Ile2, Arg4 and Cys5, respectively (Figure 6B).

Figure 3. Interaction between *Mo*-CBP$_3$-PEPIII and exo-β-(1,3)-glucanase (EXG - PDB ID 2QZW). The catalytic residues Glu192 and Glu292 of EXG are represented in yellow stick and *Mo*-CBP$_3$-PEPIII is represented as a stick and sphere colored in cyan. The docking score on the interaction was -7.0 kcal/mol. The dashed lines represent the distance in Å (small numbers) between the catalytic residues and *Mo*-CBP$_3$-PEPIII.

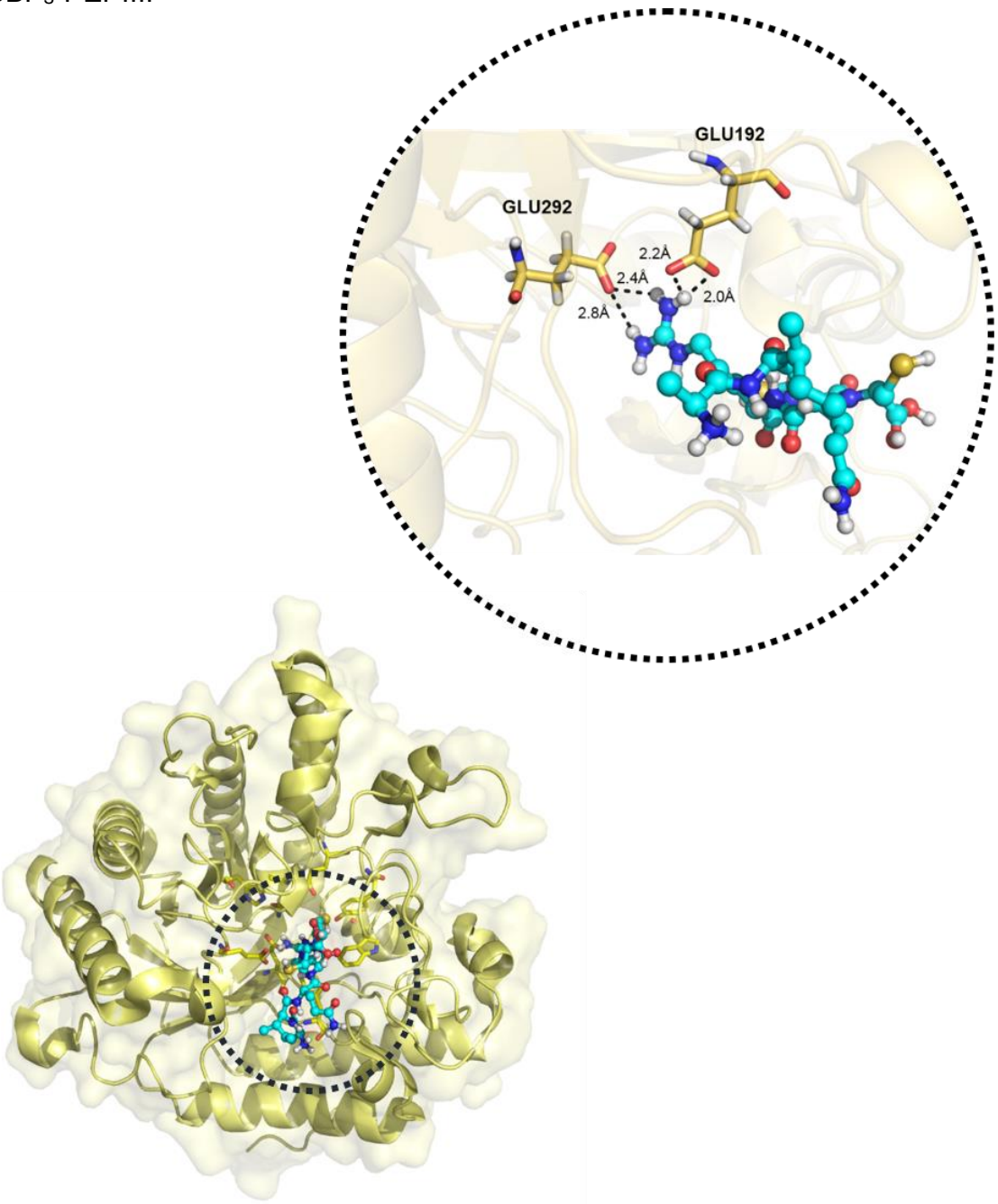

Source: Prepared by the author

Figure 4. RMSD of the complexes *Mo*-CBP$_3$-PEPIII with secreted aspartic protease 5 (SAP5) (green) and with exo-β-(1,3)-glucanase (yellow) during 20 ns of molecular dynamics.

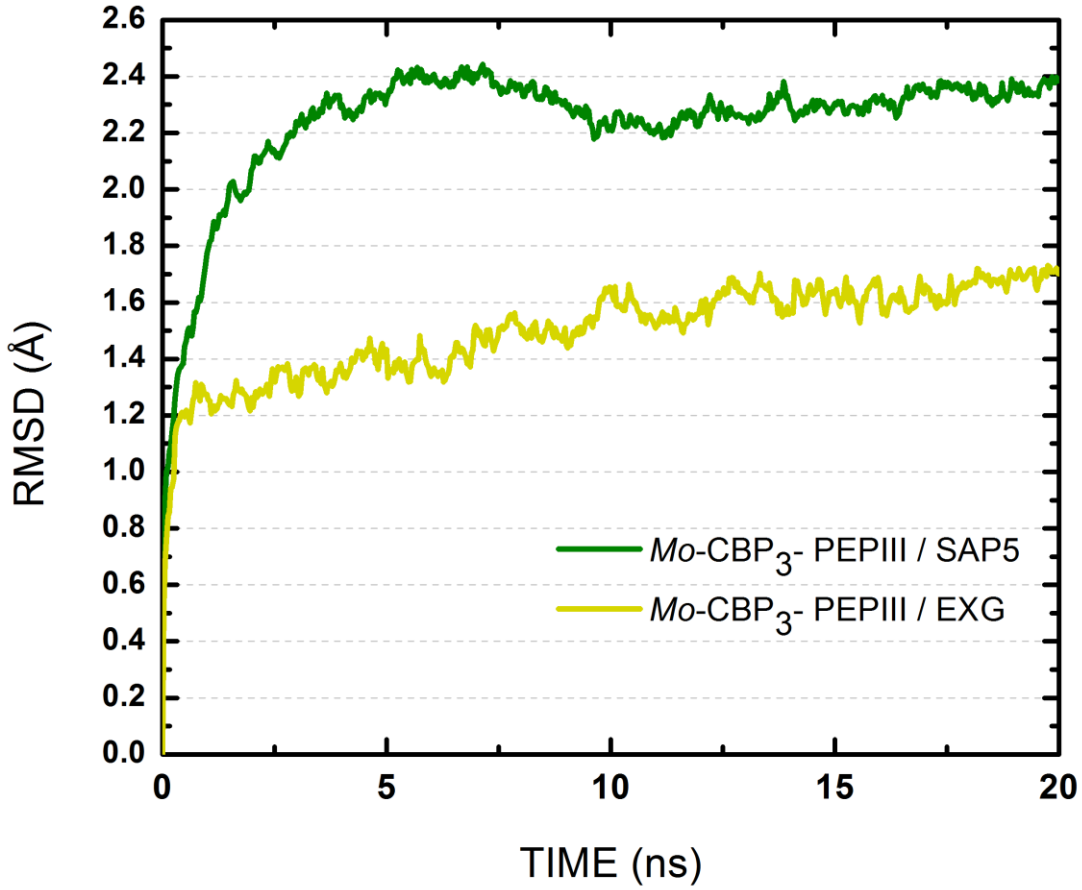

Source: Prepared by the author

The catalytic residue Asp32 from SAP5 has the third lowest energy of interaction with *Mo*-CBP$_3$-PEPIII. This energy was -16.4 kcal/mol, with a radius of 2.5 Å, and two water molecules favoring hydrogen bridges (Figure 5). The main interactions of Asp32 is with Ala1 (-14.4 kcal/mol) and Gln3 (-2.0 kcal/mol) amino acids, with distance of 2.6 Å and 4.3 Å, respectively (Figure 6C).

Figure 5. Binding site, interaction energy, and residues domain (BIRD) panel showing the MFCC interaction energy for main interactions established of the secreted aspartic protease 5 (SAP5) with *Mo*-CBP$_3$-PEPIII and with the inhibitor pepstatin. Blue and pink bars represent values obtained with *Mo*-CBP$_3$-PEPIII and pepstatin, respectively. Colored numbers at the left side of the panel assign the distance in Å between the residue of SAP5 and the ligand for each interaction. The number of water molecules involved for each interaction are presented at the right side of the panel. Numbers colored in blue and pink are related to *Mo*-CBP$_3$-PEPIII and Pepstatin residues, respectively.

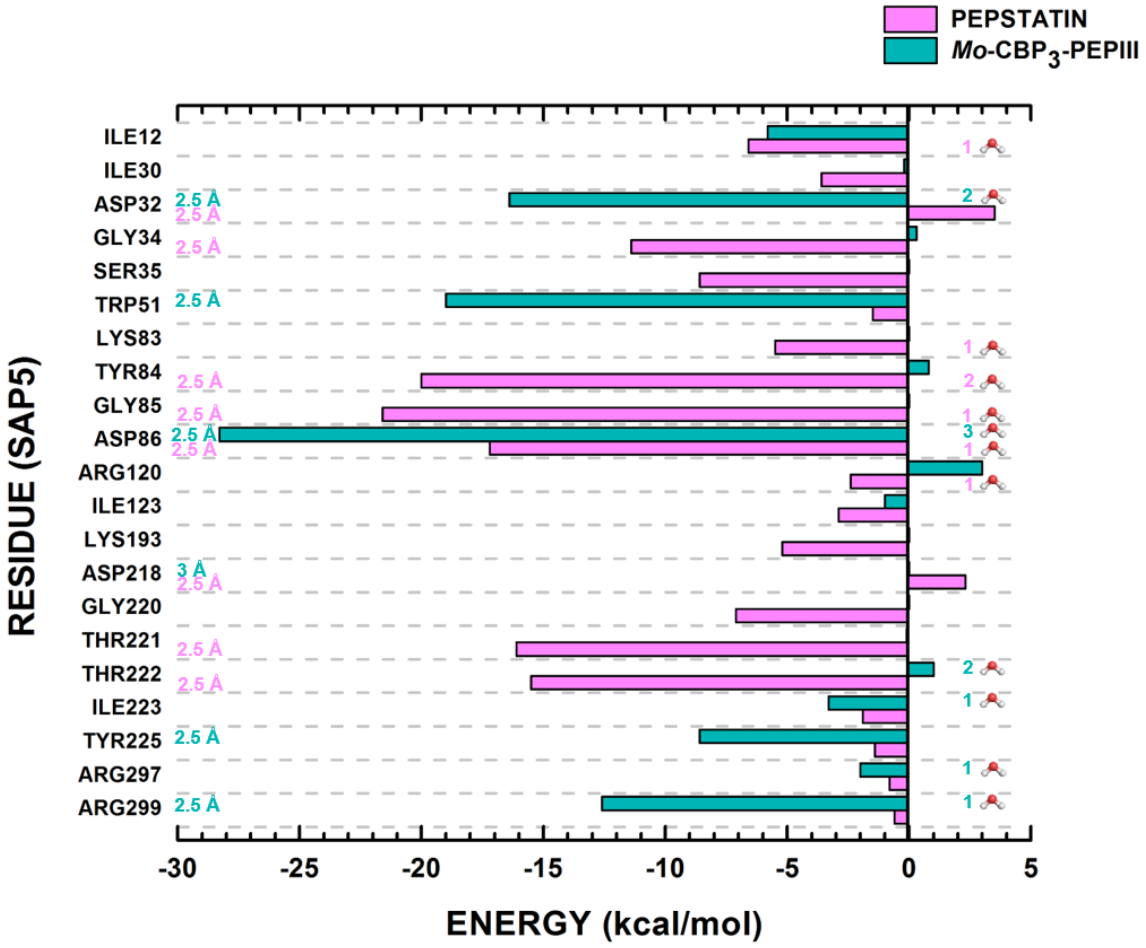

Source: Prepared by the author

Other interactions of smaller energy between the SAP5 and *Mo*-CBP$_3$-

PEPIII can be visualized in Figure 5. The interactions of residues Arg299 and Tyr225 present energy of -12.6 kcal/mol and -8.6 kcal/mol, respectively. The first one has a great attraction (-9.6 kcal/mol) by Cys6 of *Mo*-CBP$_3$-PEPIII, possessing a distance of 1.7 Å (Fig. 6D). Tyr225 presents interaction with Gln3 and Cys6 of *Mo*-CBP$_3$-PEPIII with attractive energy of -2.0 kcal/mol and -6.6 kcal/mol, respectively.

For comparison, was carried out a comparison of the SAP5 interactions parameters with pepstatin, a commercial inhibitor of aspartyl proteases. SAP5 presented more interactions with pepstatin than with *Mo*-CBP$_3$-PEPIII. However, the individual interactions with this inhibitor are lower than interaction with *Mo*-CBP$_3$-PEPIII. The residues of lower energies were different. Only the Asp86 showed large energy attractive with both ligands.

For the two catalytic residues, Asp32 and Asp218, pepstatin presented small repulsive energies, while *Mo*-CBP$_3$-PEPIII showed great attractive energy for Asp32 and null energy for Asp218. The main interactions of pepstatin with SAP5 was with the residues Gly85 (-21.6 kcal/mol), Tyr84 (-20.0 kcal/mol), Asp86 (-17.2 kcal/mol), Thr221 (-16.1 kcal/mol) and Thr222 (-15.5 kcal/mol).

The main contributions of energy in the interactions of SAP5 with *Mo*-CBP$_3$-PEPIII and with pepstatin occur in radius near of the active site. Until the radius of 3.5 Å it was observed large energy contributions, but after this distance, a stabilization in the energy was observed, which indicates that larger rays do not interfere significantly in the energies of interaction (Figure 7). It was observed that the total energy of interaction until the radius of 5 Å of SAP5 with *Mo*-CBP$_3$-PEPIII was -104.9 kcal/mol, and SAP5 with the pepstatin was -152.2 kcal/mol. This result indicates that the inhibition of the enzyme SAP5 per pepstatin is stronger than the inhibition caused by *Mo*-CBP$_3$-PEPIII.

Figure 6. Main amino acid residues involved in *Mo*-CBP$_3$-PEPIII anchorage in SAP5 enzyme. The binding site, interaction energy and residues domain (BIRD) panels placed at the left side present the MFCC interaction energy for each interaction performed by Glu86 (A), Trp51 (B), Asp32 (C), Arg299 (D) and Tyr225 (E). The residue coordinations are represented at the right side. *Mo*-CBP$_3$-PEPIII is represented as sticks and spheres colored in cyan and residues of the SAP5 are represented in green stick. The main interactions represented as black dashed lines (distances are indicated in Å). Water representations at the right side of the BIRD panels indicate interactions involving water molecules.

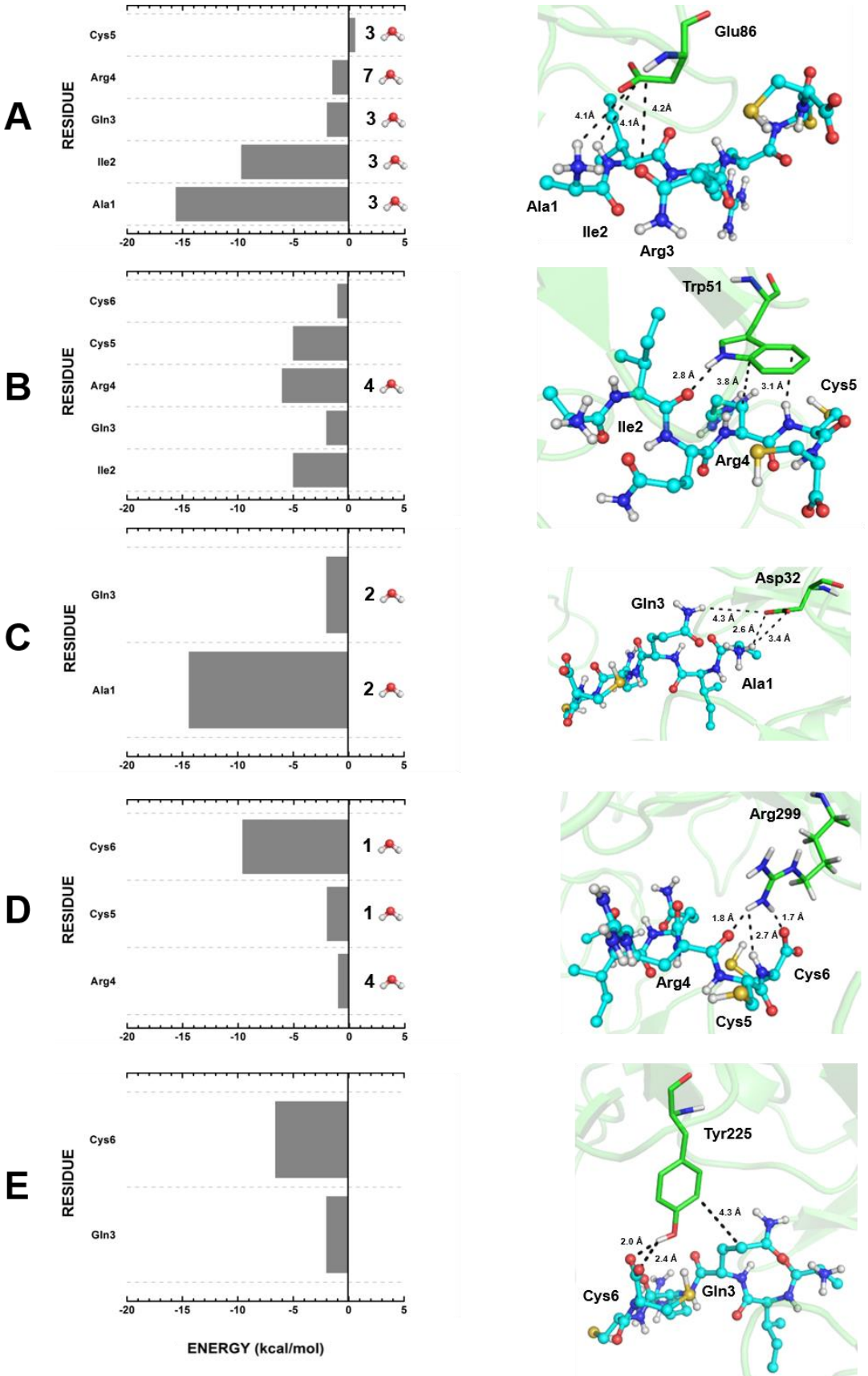

Source: Prepared by the author

2.3.4 Interaction between Mo-CBP$_3$-PEPIII and EXG

Mo-CBP$_3$-PEPIII interacts mainly with the residues Glu262, Arg309, Glu27, Glu292, Phe144, Phe258 and Tyr317 of EXG from *C. albicans*. The strongest interaction occurs with Glu262 with an energy of -16.6 kcal/mol. This interaction presents no water molecules and hydrogen bridges, and a radius of 2.5 Å (Figure 8). The great attractive energy of Glu262 is due to the interaction of its carboxylic group

Figure 7. *Mo*-CBP$_3$-PEPIII and pepstatin total interaction energy as a function of the binding pocket radius. Amino acid residues responsible for the regions of steepest negative variation are highlighted. Blue squares and pink circles represent the *Mo*-CBP3-PEPIII and pepstatin values, respectively. Et (5Å) represent the sum of energies until 5 Å and energy values are represented as kcal mol^{-1}.

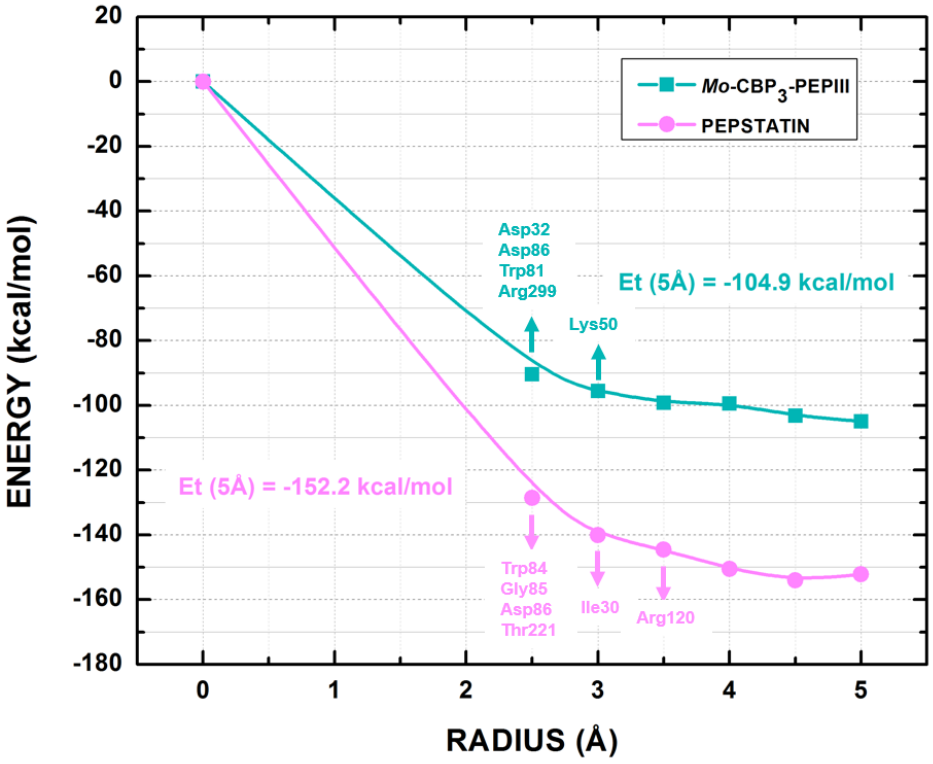

Source: Prepared by the author

of side chain with nitrogen grouping of the residue Ala1 of *Mo*-CBP$_3$-PEPIII, possessing a distance of 1.7 Å and an energy of -16.1 kcal/mol (Figure 9A). The residue Arg309 also presents a great attraction energy with the *Mo*-CBP$_3$-PEPIII, possessing a total energy of -15.3 kcal/mol. The interaction of Arg309 presents a water molecule forming hydrogen bridge and a radius of 2.5 Å (Figure 8). The energy of this residue is mainly due to the interaction of their nitrogenous group with the carboxylic group of the residue Cys6 of the *Mo*-CBP$_3$-PEPIII (Figure 9B). The Arg309 also presents a small repulsive energy through the interaction with the residue Cys5 with energy of + 0.5 kcal/mol.

The residue of Arg4 of *Mo*-CBP$_3$-PEPIII is located in a region inside the catalytic site of the enzyme, being the only residue interacting with the residue Glu27 and Glu292. Glu27 presents an energy of -15.0 kcal/mol, due to affinity of its nitrogenous group for carboxylic group of Arg4, with a distance of 1.8 Å (Figure 9C). The residue Glu292 has energy of -14.0 kcal/mol and also small distances of 1.9 Å and 2.1 Å, as shown in Figure 9D.

The residues Phe144 and Phe258 from *Mo*-CBP$_3$-PEPIII present energies of -13.9 kcal/mol and -12.8 kcal/mol, respectively. The first one interacts mainly with the EXG residues Gln3, Arg4, Cys5 and Cys6, with energies of -3.6 kcal/mol, -4.0 kcal/mol -3.0 kcal/mol and -3.1 kcal/mol, respectively. Interactions with the peptide occur through the aromatic ring present on its side chain of the residue Phe144, which has the smallest distance of 2.7 Å to EXG residue Arg4, as shown in Figure 9E. The oxygen molecule from the residue Phe258 interacts with the nitrogenous group of Ala1 peptide with energy of interaction of -6.6 kcal/mol and distance of 2 Å. The aromatic ring of the same residue interacts with the residue Arg4 of the peptide with energy of -4.0 kcal/mol and distance of 3.9 Å, as shown in Figure 9F. The main contributions of energy in the interaction between *Mo*-CBP$_3$-PEPIII and EXG are in the radii of 2.5 Å and 3.0 Å. After these radii no significant contributions in the energy are observed (Figure 10). This result indicates that amino acids in larger radius do not present significant energy, seen a convergence in the energy.

Figure 8. Binding site, interaction energy, and residues domain (BIRD) panel showing the MFCC energy for main interactions established of the exo-β-(1,3)-glucanase (EXG) with *Mo*-CBP$_3$-PEPIII and with the glucanase inhibitor castanospermine. Blue and red bars represent values obtained with *Mo*-CBP$_3$-PEPIII and castanospermine, respectively. Colored numbers at the left side of the panel assign the distance in Å between the residue of EXG and the ligand for each interaction. The number of water molecules involved for each interaction are presented at the right side of the panel. Numbers colored in blue and red are related to *Mo*-CBP$_3$-PEPIII and castanospermine residues, respectively.

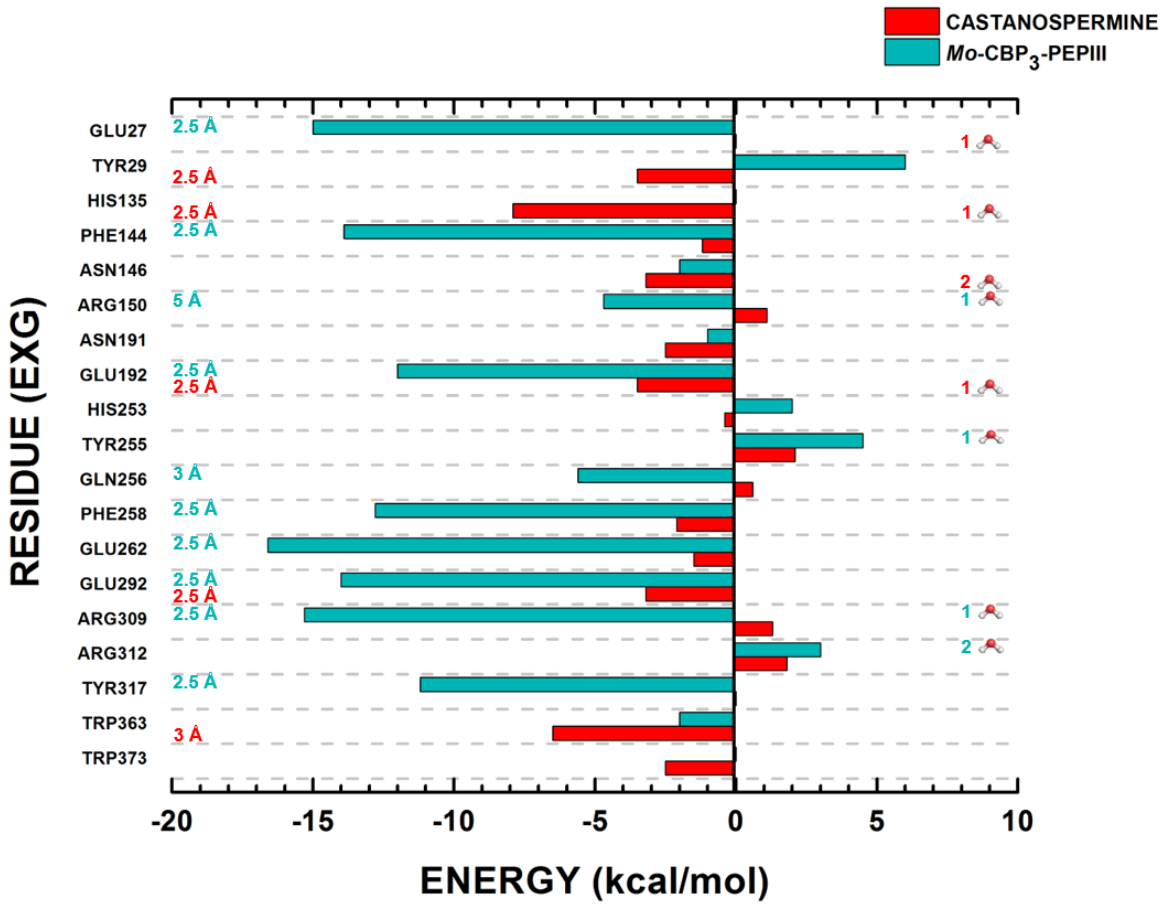

Source: Prepared by the author

The main contributions of energy in the interaction between *Mo*-CBP$_3$-PEPIII and EXG are in the radii of 2.5 Å and 3.0 Å, after these no significant contribution in the energy is observed (Figure 10). This result indicates that amino acids in larger radius not present significant energy, seen a convergence in the energy.

For effect of comparison, the calculus of energies for the commercial inhibitor castonospermine was done. The peptide *Mo*-CBP$_3$-PEPIII presents an attractive energy total of -122.2 kcal/mol for the EXG, proving to be a powerful inhibitor of this enzyme, because its inhibitor castanospermine presented a total energy of interaction of -34.9 kcal/mol until the radius of 5 Å. The main residues of interaction between castanospermine and EXG were His135, Glu192, Tyr29, being different from those observed in the interaction between EXG and *Mo*-CBP$_3$-PEPIII, such as observed in the figure 10.

2.3.5 Interaction between Mo-CBP$_3$-PEPIII and fungi membrane

The *Mo*-CBP$_3$-PEPIII is able to interact and form pores in membranes of *Candida spp*. as showed by Oliveira et al (2018). With the goal of understanding how this interaction occurs, we performed simulation of molecular dynamic between the *Mo*-CBP$_3$-PEPIII and a realistic membrane of fungus. In the simulation, we observed the interaction of the peptide *Mo*-CBP$_3$-PEPIII with the membrane along the time, as shown in Figure 11. The snapshot of the time of 0 ns shows the initial conformation of simulation, where the peptide is close the membrane, which involve water and ions. After 50 ns, we can observe the interaction of the *Mo*-CBP$_3$-PEPIII with the

Figure 9. Main amino acid residues involved in *Mo*-CBP$_3$-PEPIII anchorage in EXG enzyme. The binding site, interaction energy and residues domain (BIRD) panels placed at the left side present the MFCC interaction energy for each interaction performed by Glu262 (A), Arg309 (B), Glu27 (C), Glu292 (D), Phe144 (E) and Phe258 (F). The residue coordinations are represented at the right side. *Mo*-CBP$_3$-PEPIII is represented as sticks and spheres colored in cyan and residues of the EXG are represented in yellow stick. The main interactions represented as black dashed lines (distances are indicated in Å). Water representations at the right side of the BIRD panels indicate interactions involving water molecules.

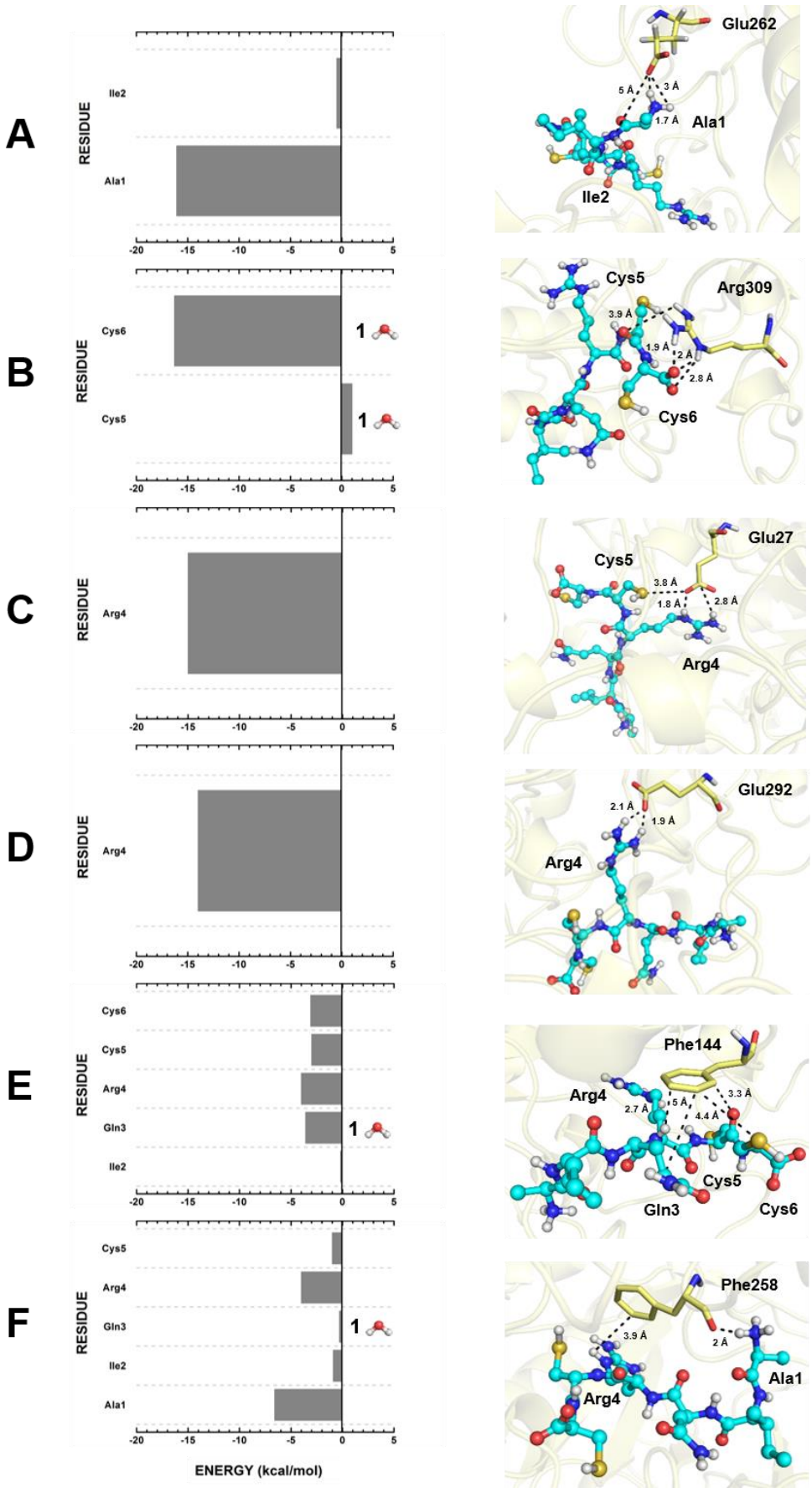

Source: Prepared by the author

Figure 10. *Mo*-CBP$_3$-PEPIII and castanospermine total interaction energy as a function of the binding pocket radius. Amino acid residues responsible for the regions of steepest negative variation are highlighted. Blue squares and red circles represent the *Mo*-CBP3-PEPIII and castanospermine values, respectively. Et (5Å) represent the sum of energies until 5 Å and energy values are represented as kcal mol^{-1}.

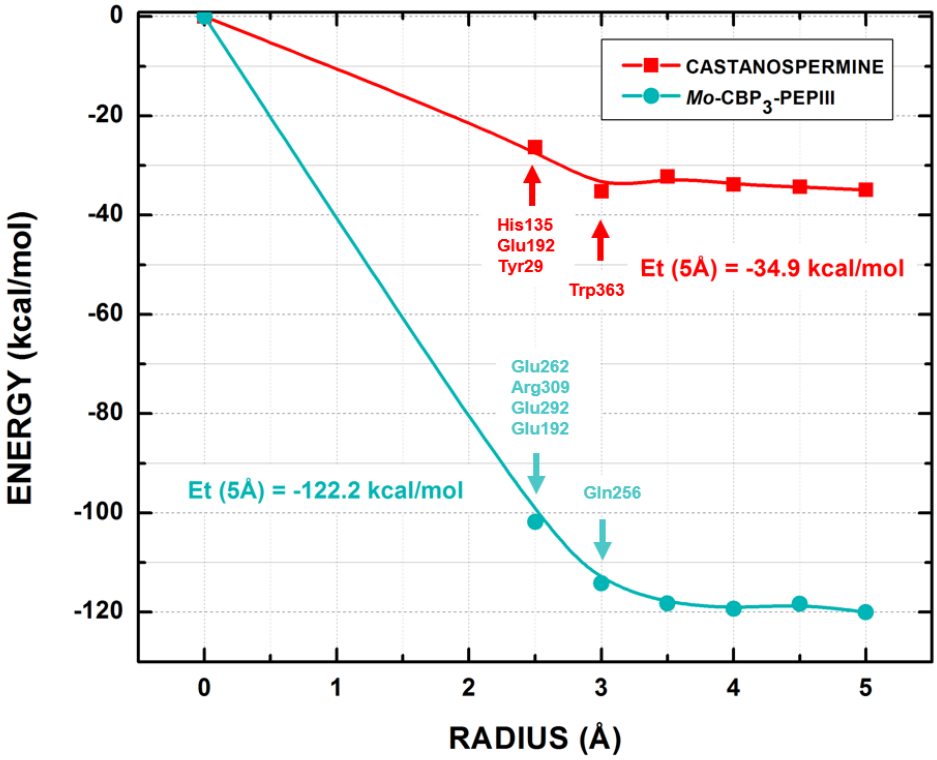

Source: Prepared by the author

superficial area of the membrane without insertion. After 100 ns it possible, indeed, visualize the insertion *Mo*-CBP$_3$-PEPIII on the membrane. With the snapshot of 150 ns it is noticed the permanence insertion of *Mo*-CBP$_3$-PEPIII on the membrane.

This result is similar to the results obtained by Yang and co-workers (2018), in which the author also analyzes the insertion of peptides in simple membranes composed of POPG: POPC. These authors demonstrated that some peptides are able to insert themselves in the membrane after approximately 100 ns. The *Mo*-CBP$_3$-PEPIII displayed a mode of interaction with the membrane very similar to that of the BAX core α5 and melittin peptide, by localizing into the sub-surface

region of the membrane, such as showed by Romero and co-workers (2017).

Figure 11. Snapshots of *Mo*-CBP$_3$-PEPIII inside realistic membrane during molecular dynamics. (A) Snapshot of 0 ns; (B) Snapshot of 50 ns; (C) Snapshot of 100 ns; (D) Snapshot of 150 ns. Color code: CHL, green; DOPC, silver; POPE, pink; POPS, cyan; POPA, purple; DPPC, lime.

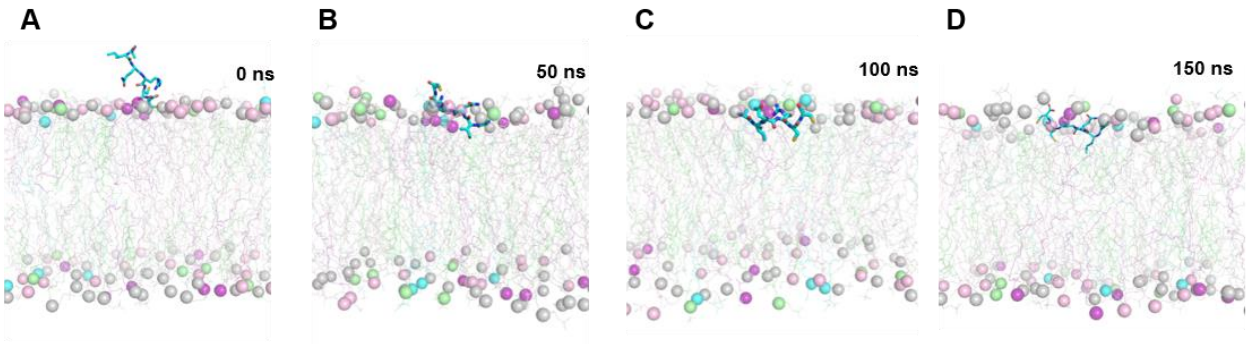

Source: Prepared by the author

3 CONCLUSION

The antimicrobial peptide *Mo*-CBP$_3$-PEPIII has a broad spectrum of action. *Mo*-CBP$_3$-PEPIII present no antifungal activity similar to the classes of the azoles. *Mo*-CBP$_3$-PEPIII obtained energy of interaction with the active site of the secreted aspartic protease 5 (SAP5) smaller than the pepstatin inhibitor. *Mo*-CBP$_3$-PEPIII possess energy of interaction with the enzyme exo-β-(1,3)-glucanase stronger than the inhibitor castanospermine, indicating its multiple mechanism of action and possessing similar action to antifungal agents of the class of echinocandins. The peptide *Mo*-CBP$_3$-PEPIII is also able to interact and enter into the sub-surface region of the fungal membranes.

REFERENCES

ÁLVARES, C. A.; SVIDZINSKI, T. I. E.; CONSOLARO, M. E. L. Candidíase vulvovaginal: fatores predisponentes do hospedeiro e virulência das leveduras. **Jornal Brasileiro de Patologia e Medicina Laboratorial,** Maringá, v. 43, n. 5, p. 319–327, 2007.

BALLIANO, L. C.; MILLA, P.; ROCCO, F.; CONZELMANN, A.; VIONNET, C.; KELLY, D. E.; KELLY, S.; SCHWEIZER, E.; SCHU, H.-J.; LLER, U. H. Systematic analysis of yeast strains with possible defects in lipid metabolism. **Yeast**, Graz, v. 15, n. 7, p. 601−614, 1999.

BARCHIESI, F.; ORSETTI, E.; OSIMANI, P.; CATASSI, C.; SANTELLI, F.; MANSO, E. Factors related to outcome of bloodstream infections due to *Candida parapsilosis* complex. **BMC Infectious Diseases,** Ancona, v. 16, n. 387, 2016.

BATISTA, A. B.; OLIVEIRA, J.T.; GIFONI, J. M.; PEREIRA, M. L.; ALMEIDA, M. G.; GOMES, V. M.; DA CUNHA, M.; RIBEIRO, S. F.; DIAS, G. B.; BELTRAMINI, L. M.; LOPES, J. L.; GRANGEIRO, T. B.; VASCONCELOS, I. M. New insights into the structure and mode of action of *Mo*-CBP3, an antifungal chitin-binding protein of *Moringa oleifera* seeds. **PLoS One**, Fortaleza, v. 9, n. 111427, 2014.

BERKOW, E. L.; LOCKHART, S. R. Fluconazole resistance in Candida species: a current perspective. **Infection and Drug Resistance,** Atlanta, v. 10, p. 237–245, 2017.

BORELLI, C.; RUGE, E.; LEE, J. H.; SCHALLER, M.; VOGELSANG, A.; MONOD, M.; KORTING, H. C.; HUBER, R.; MASKOS, K. X-ray structures of Sap 1 and Sap5: Structural comparison of the secreted aspartic proteinases from Candida albicans. **Proteins-Structure Function and Bioinformatics**, Munich, v. 72, n. 4, p. 1308-1319, 2008.

BROOKS, B.R.; BROOKS III, C.L.; MACKERELL, A.D.; NILSSON, L.; PETRELLA, R.J.; ROUX, B.; WON, Y.; ARCHONTIS, G.; BARTELS, C.; BORESCH, S.; CAFLISCH, A.; CAVES, L.; CUI, Q.; DINNER, A.R.; FEIG, M.; FISCHER, M. S.; GAO, J.; HODOSCEK M.; IM, W.; KUCZERA, K.; LAZARIDIS, T.; MA, J.; OVCHINNIKOV, V.; PACI, E.; PASTOR, R.W.; POST, C.B.; PU, J.Z.; SCHAEFER, M.; TIDOR, B.; VENABLE, R. M.; WOODCOCK, H. L.; WU, X.; YANG, W.; YORK, D.M.; KARPLUS, M. CHARMM: The Biomolecular Simulation Program. **Journal of Computational Chemistry,** Bethesda, v. 30, n. 10, p. 1545-1614, 2009.

CARDOSO, M. H.; CANDIDO, E. S.; OSHIRO, K. G. N.; REZENDE, S. B.; FRANCO, O. L. 5 – Peptides containing d-amino acids and retro-inverso peptides: General applications and special focus on antimicrobial peptides. **Peptide Applications in Biomedicine, Biotechnology and Bioengineering**, Brasília, v. 1, p. 131 –155, 2018.

CHEN, X. H.; ZHANG, Y. K.; ZHANG, J. Z. H. An efficient approach for ab initio energy calculation of biopolymers. **Journal of Chemical Physics**, New York, v. 122, n. 184105, 2005.

CUTFIELD, S. M.; DAVIES, G. J; MURSHUDOV, G.; ANDERSON, B.F.; MOODY, P. C. E.; SULLIVAN, P. A.; CUTFIELD, J. F. The structure of the exo-beta-(1,3)-glucanase from Candida albicans in native and bound forms: Relationship between a pocket and groove in family 5 glycosyl hydrolases. **Journal of Molecular Biology**, Dunedin, v. 293, n. 3, p. 771-783, 1999.

CZAPLEWSKI, L., BAX, R., CLOKIE, M., DAWSON, M., FAIRHEAD, H., FISCHETTI, V. A. Alternatives to antibiotics-a pipeline portfolio review. **Lancet Infectious Diseases,** Abingdon, v. 16, n. 2, p. 239–251, 2016.

DELLEY, B. From molecules to solids with the DMol3 approach. **The Journal of Chemical Physics**, Villigen, v. 113, p. 7756-7764, 2000.

FJELL, C. D.; HISS, J. A.; HANCOCK, R. E. W.; SCHNEIDER, G. Designing antimicrobial peptides: form follows function. **Nature Reviews Drug Discovery**, Vancouver, v. 11, n. 1, p. 124-124, 2012.

FLORES-ROMERO, H.; GARCIA-PORRAS, M.; BASAÑEZ, G. Membrane insertion of the BAX core, but not latch domain, drives apoptotic pore formation. **Scientific Reports**, Leioa, v. 7, n. 16259, 2017.

FOSGERAU, K.; HOFFMANN, T. Peptide therapeutics: current status and future directions. **Drug Discovery Today**, Copenhagen, v. 20, p. 122-128, 2015.

FRANCOIS, I.E.; AERTS, A.M.; CAMMUE, B.P.; THEVISSEN, K. Currently used antimycotics: spectrum, mode of action and resistance occurrence. **Current Drug Targets,** Heverlee, v. 6, n. 8, p. 895-907, 2005.

FREIRE, J.E.; VASCONCELOS, I.M.; MORENO, F.B.; BATISTA, A.B.; LOBO, M. D.; PEREIRA, M. L.; LIMA, J. P.; ALMEIDA, R. V.; SOUSA, A. J.; MONTEIRO-MOREIRA, A. C.; OLIVEIRA, J. T.; GRANGEIRO, T.B. *Mo*-CBP3, an antifungal chitin-binding protein from *Moringa oleifera* seeds, is a member of the 2S albumin family. **PLoS One**, Fortaleza, v. 10, n. 0119871, 2015.

HANCOCK, R. E. W.; SAHL, H. G. Antimicrobial and host-defense peptides as new anti-infective therapeutic strategies. **Nature Biotechnology**, Vancouver, v. 24, n. 12, p. 1551-1557, 2006.

HE, X.; ZHANG, J. Z. H. A new method for direct calculation of total energy of protein. **Journal of Chemical Physics**, Nanjing, v. 122, n. 031103, 2005.

IKONOMOVA, S. P.; MOGHADDAM-TAAHERI, P.; JABRA-RIZK, M. A.; WANG, Y.; KARLSSON, A. J. Engineering improved variants of the antifungal peptide histatin 5 with reduced susceptibility to Candida albicans secreted aspartic proteases and enhanced antimicrobial potency. **The FEBS Journal,** College Park v. 285, n. 1, p. 146–159, 2018.

JO, S.; KIM, T.; IM, W. Automated Builder and Database of Protein/Membrane

Complexes for Molecular Dynamics Simulations. **PLoS ONE***,* Lawrence*,* v. 2, n. 9, 2007.

JO, S.; KIM, T.; IYER, V.G.; IM, W. CHARMM-GUI: A Web-based Graphical User Interface for CHARMM. **Journal of Computational Chemistry,** Lawrence, v. 29, n. 11, p. 1859-1865, 2008.

LEE, J.; CHENG, X.; SWAILS, J.M.; YEOM, M.S.; EASTMAN, P.K.; LEMKUL, J.A.; WEI, S.; BUCKNER, J.; JEONG, J.C.; QI, Y.; JO, S.; PANDE, V.S.; CASE, D.A.; BROOKS III, C.L.; MACKERELL JR, A.D.; KLAUDA, J.B.; IM, W. CHARMM-GUI Input Generator for NAMD, GROMACS, AMBER, OpenMM, and CHARMM/OpenMM Simulations using the CHARMM36 Additive Force Field. **Journal of Chemical Theory and Computation,** Lawrence, v. 12, n. 1, p. 405-413, 2016.

LEE, J.; PATEL, D.S.; STÅHLE, J.; PARK, S-J.; KERN, N.R.; KIM, S.; LEE, J.; CHENG, X.; VALVANO, M.A.; HOLST, O.; KNIREL, Y.; QI, Y.; JO, S.; KLAUDA, J.B.; WIDMALM, G.; IM, W. CHARMM-GUI Membrane Builder for Complex Biological Membrane Simulations with Glycolipids and Lipoglycans. **Journal of Chemical Theory and Computation**, Bethlehem, v. 15, n.1, p. 775-786, 2019.

LUM, K. Y.; TAY, S. T.; LE, C. F.; LEE, V. S.; SABRI, N. H.; VELAYUTHAN, R. D.; HASSAN, H.; SEKARAN, S. D. Activity of Novel Synthetic Peptides against Candida albicans. **Scientific Reports**, Kuala Lumpur, v. 5, n. 9657, 2015.

LYU, Y.; XIANG, N.; MONDAL, J.; ZHU, X.; NARSIMHAN, G. Characterization of Interactions between Curcumin and Different Types of Lipid Bilayers by Molecular Dynamics Simulation. **Journal of Physical Chemistry B**, West Lafayette, v. 122, n. 8, p. 2341-2354, 2018.

MAHLAPUU, M.; HÅKANSSON, J.; RINGSTAD, L.; & BJÖRN, C. Antimicrobial peptides: an emerging category of therapeutic agents**. Frontiers in Cellular and Infection Microbiology**, Solna, v. 6, n. 194. 2016.

MATHÉ, L.; VAN DIJCK, P. Recent insights into *Candida albicans* biofilm resistance mechanisms. **Current Genetics,** Leuven v. 59, n. 4, p. 251-264, 2013.

MAUBON, D.; GARNAUD, C.; CALANDRA, T.; SANGLARD, D.; CORNET, M. Resistance of Candida spp. to antifungal drugs in the ICU: where are we now? **Intensive Care Medicine,** Grenoble, v. 40, n. 9, p. 1241-1255, 2014.

MAYER, L. F.; WILSON, D. & HUBE, B. *Candida albicans* pathogenicity mechanisms. **Virulence**, Jena, v. 4, n.2, p. 119 –128, 2013.

MESA-ARANGO, A.C.; SCORZONI, L.; ZARAGOZA, O. It only takes one to do many jobs: Amphotericin B as antifungal and immunomodulatory drug. **Frontiers in Microbiology**, Madrid, v. 3, p. 286, 2012.

NEGRI M.; MARTINS M.; HENRIQUES M.; SVIDZINSK T.I.; AZEREDO J.; OLIVEIRA R. Examination of potential virulence factors of *Candida tropicalis* clinical

isolates from hospitalized patients. **Mycopathologia**, Braga, v. 82, n. 3, p. 169-175, 2010.

NETT, J.E.; ANDES, D.R. Antifungal agents: spectrum of activity, pharmacology, and clinical indications. **Infectious Disease Clinics of North America,** Madison, v. 30, n. 1, p. 51-83, 2016.

OLIVEIRA, J. T. A.; SOUZA, P. F. N.; VASCONCELOS, I.M.; DIAS, L.P.; MARTINS, T.F.; VAN TILBURG, M.F.; GUEDES, M. I. F.; SOUSA, D. O. B. Mo-CBP3-PepI, Mo-CBP3-PepII, and Mo-CBP3-PepIII are synthetic antimicrobial peptides active against human pathogens by stimulating ROS generation and increasing plasma membrane permeability. **Biochimie**, Fortaleza, v. 157, p. 10-21, 2018.

PAPPAS, P.G.; KAUFFMAN, C.A.; ANDES, D.R.; CLANCY, C.J.; MARR, K.A.; OSTROSKY-ZEICHNER, L.; REBOLI, A.C.; SCHUSTER, M.G.; VAZQUEZ, J. A.; WALSH, T. J.; ZAOUTIS, T.E.; SOBEL, J.D. Clinical practice guideline for the management of candidiasis: 2016 update by the infectious diseases society of america. **Clinical Infectious Disease,** Birmingham, v. 62, n. 4, p. 1-50, 2016.

PARAMYTHIOTOU, E.; FRANTZESKAKI, F.; FLEVARI, A.; ARMAGANIDIS, A.; DIMOPOULOS, G. Invasive fungal infections in the ICU: how to approach, how to treat. **Molecules**. Haidari, v. 19, p. 1085-1119, 2014.

PATIL, S.; RAO, R.S.; MAJUMDAR, B.; ANIL, S. Clinical appearance of oral candida infection and therapeutic strategies. **Frontiers in Microbiology,** Bangalore, v. 6, n. 1391, 2015.

PHILLIPS, J. C.; BRAUN, R.; WANG, W.; GUMBART, J.; TAJKHORSHID, E.; VILLA, E.; CHIPOT, C.; SKEEL, R. D.; KALE, L.; SCHULTEN, K. Scalable molecular dynamics with NAMD. **Journal of Computational Chemistry**, Urbana, v. 26, n. 16, p. 1781-1802, 2005.

PRASAD, R.; SHAH, A. H.; RAWAL, M. K. Antifungals: mechanism of action and drug resistance. **Yeast Membrane Transporter Advances in Experimental Medicine and Biology**, New Delhi, v. 892, p. 327–349, 2016.

PUIG-ASENSIO, M.; PEMAN, J.; ZARAGOZA, R.; GARNACHO-MONTERO, J.; MARTIN-MAZUELOS, E. CUENCA-ESTRELLA, M.; ALMIRANTE, B. Impact of Therapeutic Strategies on the Prognosis of Candidemia in the ICU. **Critical Care Medicine**, Barcelona, v. 42, p. 1423-1432, 2014.

QUINDÓS, G. Epidemiology of candidaemia and invasive candidiasis. A changing face. **Revista Iberoamericana de Micología,** Bilbao, v. 31, p. 42–48, 2014.

RODRIGUES, C. R. F.; OLIVEIRA, J. I. N.; FULCO, U. L.; ALBUQUERQUE, E. L.; MOURA, R. M.; CAETANO, E. W. S.; FREIRE, V. N. Quantum biochemistry study of the T3-785 tropocollagen triple-helical structure. **Chemical Physics Letters**, Natal, v. 559, p. 88-93, 2013.

SCHNEIDER, J.; MATEO, E.; MARCOS-ARIAS, C.; EIRO, N.; VIZOSO, F.; PÉREZ-FERNÁNDEZ, R.; ERASO, E.; QUINDÓS, G. Antifungal activity of the human uterine cervical stem cells conditioned medium (hUCESC-CM) against Candida albicans and other medically relevant species of Candida. **Frontiers in Microbiology**, Gijón, v. 9, n. 2818, 2018.

SHOHAM, S.; MARR, K.A. Invasive fungal infections in solid organ transplant recipients. **Future Microbiology,** Baltimore, v. 7, n. 5, p. 639-655, 2012.

SILVA, D.R.; SARDI, J.C.O.; FREIRES, I.A.; SILVA, A.C.B.; ROSALEN, P.L. *In silico* approaches for screening molecular targets in *Candida albicans*: A proteomic insight into drug discovery and development. **European Journal of Pharmacology,** Piracicaba, v. 842, p. 64-69, 2019.

SOUSA, B. L.; BARROSO-NETO, I. L.; OLIVEIRA, E. F.; FONSECA, E.; LIMA-NETO, P.; LADEIRA, L. O.; FREIRE, V. N. Explaining RANKL inhibition by OPG through quantum biochemistry computations and insights into peptide- design for the treatment of osteoporosis. **RSC Advances**, Fortaleza, v. 6, p. 84926-84942, 2016.

TROTT, O.; OLSON, A. J. (2010), AutoDock Vina: Improving the speed and accuracy of docking with a new scoring function, efficient optimization, and multithreading. **Journal of Computational Chemistry**, La Jolla, v. 31, n. 2, p. 455-461, 2010.

WU E.L.; MEI Y.; HAN K.; ZHANG J. Z. Quantum and molecular dynamics study for binding of macrocyclic inhibitors to human alpha-thrombin. **Biophysical Journal**, Dalian, v. 92, p. 4244-4253, 2007.

WU, E.L.; CHENG, X.; JO, S.; RUI, H.; SONG, K.C.; DÁVILA-CONTRERAS, E.M.; QI, Y.; LEE, J.; MONJE-GALVAN, V.; VENABLE, R.M.; KLAUDA, J.B.; IM, W. CHARMM-GUI Membrane Builder Toward Realistic Biological Membrane Simulations. **Journal of Computational Chemistry,** Lawrence, v. 35, p. 1997-2004*,* 2014.

YANG, R.; ZHANG, G. J.; ZHANG, F. R.; LI, Z. J.; HUANG, C. Membrane permeabilization design of antimicrobial peptides based on chikungunya virus fusion domain scaffold and its antibacterial activity against gram-positive *Streptococcus pneumoniae* in respiratory infection. **Biochimie**, Zhengzhou, v. 146, p. 139-147, 2018.

ZANATTA, G.; NUNES, G. D.; BEZERRA, E. M.; DA COSTA, R. F.; MARTINS, A.; CAETANO, E. W. S.; FREIRE, V. N.; GOTTFRIED, C. Two Binding Geometries for Risperidone in Dopamine D3 Receptors: Insights on the Fast-Off Mechanism through Docking, Quantum Biochemistry, and Molecular Dynamics Simulations. **ACS Chemical Neuroscience**, Porto Alegre, v. 7, p. 1331-1347, 2016.

ZHANG, D. W.; ZHANG, J. Z. H. Molecular fractionation with conjugate caps for full quantum mechanical calculation of protein-molecule interaction energy. **Journal of Chemical Physics**, New York, v. 119, p. 3599-3605, 2003.

ANEXO A - INDIVIDUAL CONTRIBUTIONS OF AMINO ACID RESIDUES

Table S1. Individual contributions of amino acid residues to the interaction of SAP5 with *Mo*-CBP$_3$-PEPIII.

Residue		Energy	Residue		Energy
SAP5	***Mo*-CBP$_3$-PEPIII**	**(kcal/mol)**	**SAP5**	***Mo*-CBP$_3$-PEPIII**	**(kcal/mol)**
ILE12	ALA1	0.2	ASP218	GLN3	0
THR13	ALA1	-0.3	GLY220	GLN3	0
ILE30	ALA1	-0.7	THR221	GLN3	0
ASP32	ALA1	-14.4	THR222	GLN3	1
GLY34	ALA1	0.3	ILE223	GLN3	-3
TYR84	ALA1	0.8	TYR225	GLN3	-2
ASP86	ALA1	-15.6	ARG299	GLN3	0
SER88	ALA1	-0.1	ILE12	ARG4	-3
ALA119	ALA1	0.5	TRP51	ARG4	-6
ARG120	ALA1	2.3	ARG52	ARG4	0
ILE123	ALA1	-1	GLY53	ARG4	0
GLY220	ALA1	0	ASP54	ARG4	-4
THR221	ALA1	-0.1	ASP86	ARG4	-1.5
THR222	ALA1	0	ARG120	ARG4	3
ILE12	ILE2	-2	THR222	ARG4	0
THR13	ILE2	-1	ILE223	ARG4	-1
ILE30	ILE2	0.5	TYR225	ARG4	0
LYS50	ILE2	-2	ARG297	ARG4	-2
TRP51	ILE2	-5	ARG299	ARG4	-1
ASP54	ILE2	0.2	TRP51	CYS5	-5
ASP86	ILE2	-9.7	ARG52	CYS5	-1
SER88	ILE2	-1.7	ASN249	CYS5	-1
SER118	ILE2	-0.9	ARG299	CYS5	-2
ALA119	ILE2	-1.4	TRP51	CYS6	-1
ARG120	ILE2	-2.3	ASP86	CYS6	0.5
ILE12	GLN3	-1	ILE223	CYS6	0.7
ASP32	GLN3	-2	TYR225	CYS6	-6.6
TRP51	GLN3	-2	ARG299	CYS6	-9.6
ASP86	GLN3	-2			

Source: Prepared by the author

Table S2. Individual contributions of amino acid residues to the interaction of SAP5 with pepstatin.

Residue		Energy	Residue		Energy
SAP5	**Pepstatin**	**(kcal/mol)**	**SAP5**	**Pepstatin**	**(kcal/mol)**
ILE12	IVA001	-3.1	THR33	STA004	2
TRP51	IVA001	0	GLY34	STA004	-8.4
ASP86	IVA001	-0.2	SER35	STA004	-4.6
THR222	IVA001	-4	LYS83	STA004	-2.2
ILE223	IVA001	-1.3	TYR84	STA004	-13.4
TYR225	IVA001	-0.6	GLY85	STA004	-9
ARG297	IVA001	-0.8	ASP86	STA004	2
ARG299	IVA001	-0.6	SER88	STA004	-0.3
ILE12	VAL002	-3.5	ALA119	STA004	1.1
THR13	VAL002	0	ARG120	STA004	-1.4
ILE30	VAL002	-1.1	ILE123	STA004	-2.9
TRP51	VAL002	-1.5	LEU216	STA004	-1.1
ASP86	VAL002	-10.2	ASP218	STA004	4.2
SER88	VAL002	0.3	GLY220	STA004	-3.4
ARG120	VAL002	-1	THR221	STA004	-2
GLY220	VAL002	-1.4	ILE305	STA004	-0.1
THR221	VAL002	-8.1	ASP32	ALA005	1
THR222	VAL002	-9.2	GLY34	ALA005	-3
ILE223	VAL002	-0.6	SER35	ALA005	-4
TYR225	VAL002	0.2	SER36	ALA005	0
TYR84	VAL003	-2	ILE82	ALA005	-1
GLY85	VAL003	-9	LYS83	ALA005	0
ASP86	VAL003	-8.8	TYR84	ALA005	-5
GLY87	VAL003	0	GLY85	ALA005	-3
SER88	VAL003	0	GLY131	ALA005	0
LEU216	VAL003	-0.8	ALA133	ALA005	0
ASP218	VAL003	-1.9	LYS193	ALA005	-1
GLY220	VAL003	-2.3	ILE82	STA006	-1.9
THR221	VAL003	-6	LYS83	STA006	-3.3
THR222	VAL003	-2.3	TYR84	STA006	0.4
ILE223	VAL003	0	GLY85	STA006	-0.6
TYR225	VAL003	-1	GLY87	STA006	-0.3
ILE305	VAL003	-2	GLY131	STA006	-0.1
THR13	STA004	-0.6	LYS192	STA006	-3.3
ILE30	STA004	-2.5	LYS193	STA006	-4.2
ASP32	STA004	2.5			

Source: Prepared by the author

Table S3. Individual contributions of amino acid residues to the interaction of EXG with *Mo*-CBP$_3$-PEPIII.

Residue		Energy	Residue		Energy
EXG	***Mo*-CBP$_3$-PEPIII**	**(kcal/mol)**	**EXG**	***Mo*-CBP$_3$-PEPIII**	**(kcal/mol)**
PHE229	ALA1	0.5	TYR255	ARG4	14
TYR255	ALA1	-9.5	PHE258	ARG4	-4
GLN256	ALA1	-5.6	GLU292	ARG4	-14
VAL257	ALA1	-0.2	ASN305	ARG4	-1
PHE258	ALA1	-6.6	ARG312	ARG4	3
SER259	ALA1	-3.3	TYR317	ARG4	0
GLU262	ALA1	-16.1	TRP363	ARG4	-2
PHE144	ILE2	-0.2	TRP373	ARG4	0
LEU194	ILE2	-1.5	GLU27	CYS5	0
PRO196	ILE2	-0.8	TYR29	CYS5	0
PHE229	ILE2	-1.3	GLY143	CYS5	-1
PHE258	ILE2	-0.9	PHE144	CYS5	-3
SER259	ILE2	-0.2	ASP145	CYS5	-2
GLU262	ILE2	-0.5	ASN146	CYS5	0
PHE144	GLN3	-3.6	ARG150	CYS5	0
LEU194	GLN3	-0.4	PHE258	CYS5	-1
PRO196	GLN3	-0.9	LEU304	CYS5	0
PHE229	GLN3	0	ASN305	CYS5	1
PHE258	GLN3	-0.3	GLY306	CYS5	-2
SER259	GLN3	-1	ARG309	CYS5	1
TYR317	GLN3	-1.3	TYR317	CYS5	-1
GLU27	ARG4	-15	GLY143	CYS6	-0.1
TYR29	ARG4	6	PHE144	CYS6	-3.1
HSD135	ARG4	0	ASP145	CYS6	3.6
PHE144	ARG4	-4	ARG150	CYS6	-4.7
ASN146	ARG4	-2	LEU194	CYS6	-0.2
ASN191	ARG4	-1	ASN305	CYS6	0.2
GLU192	ARG4	-12	ARG309	CYS6	-16.3
LEU194	ARG4	-1	TYR317	CYS6	-8.9
HSD253	ARG4	2			

Source: Prepared by the author

Table S4. Individual contributions of amino acid residues to the interaction of EXG with castanospermine.

Residue		Energy	Residue		Energy
EXG	**Castanospermine**	**(kcal/mol)**	**EXG**	**Castanospermine**	**(kcal/mol)**
GLU27	-	0	GLU188	-	-2.1
TYR29	-	-3.5	ASP299	-	-2.3
HIS135	-	-7.9	GLY306	-	-0.1
ASN146	-	-3.2	PHE362	-	-0.7
ASN191	-	-2.5	LEU20	-	0.2
GLU192	-	-3.5	ILE95	-	-0.2
TYR255	-	2.1	TRP98	-	0
PHE258	-	-2.1	LEU194	-	0
GLU292	-	-3.2	ALA295	-	0
TRP373	-	-2.5	THR298	-	-0.7
LEU304	-	-2.4	ARG312	-	1.8
TRP363	-	-6.5	VAL361	-	-0.6
ARG92	-	3	TRP23	-	-0.4
PHE144	-	-1.2	THR31	-	-0.2
HIS253	-	-0.4	LEU134	-	-0.1
MET30	-	-0.5	GLY143	-	0
ASN142	-	-0.4	LEU190	-	0.1
PHE229	-	0.1	PRO193	-	-0.5
SER294	-	-0.3	HIS252	-	-0.1
PRO94	-	0	LYS366	-	0.6
ASP133	-	-0.5	ALA370	-	-0.2
ASP145	-	-0.5	GLU372	-	0
VAL257	-	-0.6	PHE24	-	0.2
GLY21	-	-0.1	ILE93	-	0.3
GLY22	-	-0.1	GLY96	-	-0.3
VAL25	-	-0.3	TRP131	-	0.2
SER147	-	-0.6	SER140	-	0.4
TRP293	-	-0.8	ARG150	-	1.1
SER364	-	-0.6	ARG309	-	1.3
ASN19	-	0.1	TRP365	-	-0.2
HIS254	-	0.1	TRP74	-	0.2
ASN305	-	-1	LEU149	-	-0.1
HIS226	-	-0.5	ASP227	-	-1.6
GLY291	-	-0.4	ALA228	-	0.5
ALA296	-	-0.2	SER259	-	0.1
GLN141	-	-0.1	GLU262	-	-1.5
GLY148	-	0	LEU263	-	-0.3
ASP251	-	-2	TRP277	-	0.4
GLN256	-	0.6	ALA290	-	0.1
ALA301	-	-0.3	LYS302	-	0.7
TRP303	-	0.4	VAL307	-	-0.5
THR367	-	0.2	TYR346	-	-0.2
LEU26	-	0.1	GLN350	-	-0.1
PRO28	-	0.6	SER374	-	0.1
GLY136	-	-0.3			

Source: Prepared by the author